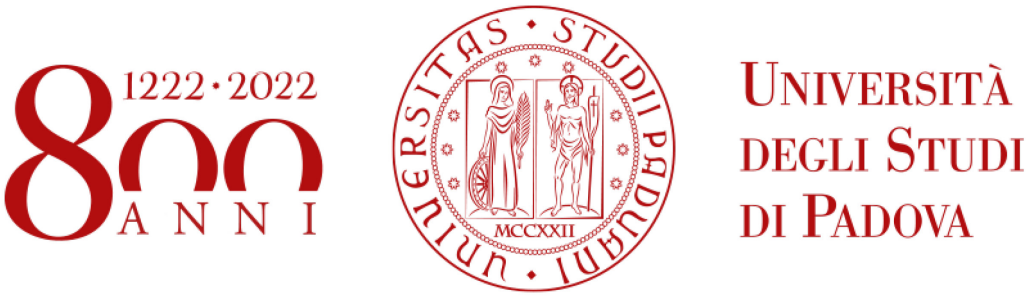

UNIVERSITÀ DEGLI STUDI DI PADOVA

DIPARTIMENTO DI SCIENZE CHIMICHE

CORSO DI LAUREA MAGISTRALE IN CHIMICA

TESI DI LAUREA MAGISTRALE

Novel graphene derivatives as sustainable materials for carbocatalysis

Relatore:
Prof. Stefano Agnoli

Controrelatore:
Prof. Fabrizio Mancin

Laureando:
Giacomo De Crescenzo

Anno Accademico 2021/2022

Table of contents

1. Purpose of the work

The concepts of environmental protection and sustainability are at the center of current national and international properties as demonstrated by the action taken in the Italian PNRR, the European Green Deal and 17 UN sustainability development goals. Recent events demonstrated that the climatic changes and fossil fuel shortage have a strong impact on everybody's life at different levels and that some decisive action must be taken in order to stop, or at least slow down, the environmental crisis our generation is set to face in the near future. In the last couple of decades, a new awareness towards sustainability has emerged also in chemical research, which has radically changed its way of thinking to meet both economic and environmental goals simultaneously. The so called Green Chemistry was first defined at the beginning of the 1990's as "the design of chemical products and processes to reduce or eliminate the use and generation of hazardous substances"[1], and its guiding framework can be summarized in the Twelve Principles introduced by Paul Anastas and John Warner in 1998[2]. These green chemistry principles have been the foundation of this thesis.

For example, the 9th principle of Green Chemistry states that catalytic processes, as selective as possible, have to be preferred to stoichiometric reactions, as catalysts speed up the kinetics and allows the use of lower temperatures. In this context, the main focus of this thesis is carbocatalysis, i.e. the use of carbon-based materials like graphene and its derivatives as heterogeneous catalysts. The sustainable and cheap syntheses of such materials poses important challenges, since most preparation routes reported in the literature employ extreme conditions of temperature (pyrolysis) or make use of sophisticated techniques and reagents with limited availability or high toxicity, like the strong oxidants employed for the production of graphene oxide.

Moreover, the catalytic reactions explored are oxidations, which are generally carried out by harmful reagents, at high temperatures or using toxic metal-based catalysts.

In this work we were able to overcome these challenges and synthesize a functionalized graphene derivative, the graphene acetic acid (GAA) and exploiting a procedure that makes limited use of harmful reagents and proceeds at relative low temperatures compared to other similar synthesis. Interestingly, GAA was investigated as catalysts for a variety of reaction and was found out to be active for two oxidation reactions: a) the oxidative homocoupling of amines to imines, which has been carried in neat conditions using the molecular oxygen present in the air as the final oxidant, and b) the oxidation of thioanisole to the corresponding sulfoxide, at room temperature, using 30% hydrogen peroxide as oxidant. In both cases, very high selectivity and recyclability were achieved.

2. Introduction

2.1 Graphene and its functionalization

2.1.1 Pristine graphene

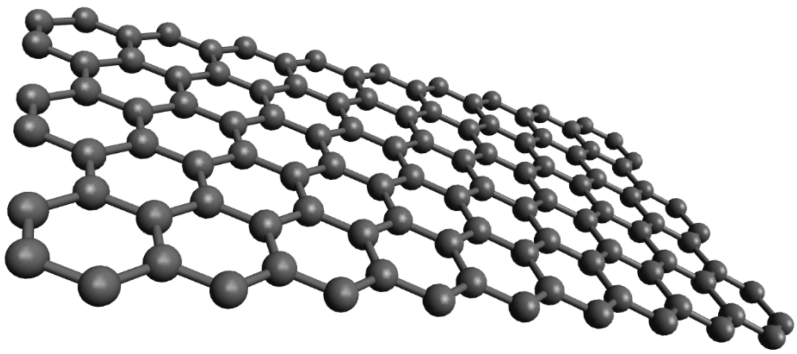

Fig. 1: Ball and stick model of a graphene layer.

Graphene is a two-dimensional, single layer arrangement of sp^2 hybridized carbon atoms. If stacked on top of each other, the graphene layers form the well-known graphite, but graphene can be also considered the building block for other allotropes such as fullerenes and carbon nanotubes. The honeycomb structure of graphene sheets, made up by sp^2 C atoms involved in long range π-conjugation yield outstanding thermal[3], mechanical[4] and electronic[5] properties, which make this material suitable for a variety of industrial applications[6] and electronic devices[7]. For these reasons, there has been an explosion of interest in this material, which led to Andrei Geim and Konstantin Novoselov being awarded the 2010 Nobel prize in Physics "for groundbreaking experiments regarding the two-dimensional material graphene". In 2004[8], in the first pioneering experiments, graphene was prepared by mechanical exfoliation (repeated peeling with Scotch tape) of small mesas of highly pyrolytic graphite. This deceptively simple way of preparing this material is in reality quite tricky, as in most experiments a number of very thick slabs is produced, which

makes the location and isolation of a single layer of graphene extremely difficult for the unexperienced. Other methods of single-layer (SLG) and few-layer graphene (FLG) preparation include, but are not limited to, electrochemical exfoliation[9], pyrolysis of silicon carbide (SiC)[10] and Chemical Vapor Deposition (CVD)[11], which is to this day the synthetical technique of choice for high-quality graphene on large scale basis[12].

Given the extraordinary physical properties of single layer graphene, there has been an increasing interest in investigating functionalization of the basal plane and edges of this material. In fact, single layers of pristine graphene have a strong tendency to agglomerate in solvents because of the many π-π intra-layer interactions, rendering very difficult the exploitation of graphene unique properties in wet-chemistry. On the other hand, the functionalization of graphene aids the dispersion the material in hydrophilic or hydrophobic media[13]. Moreover, modification of graphene using functional groups can lead to other applications, such as the use in heterogeneous catalysis as described in this thesis.

2.1.2 Functionalization of graphene and graphene oxide (GO)

The first chemically functionalized graphene was graphene oxide (GO) recognized as such in 2006[14], and isolated via exfoliation of graphite oxide. Graphene oxide sheets bear many oxygenated functions, as hydroxyls, epoxides, carboxylic acids and carbonyls which lead to the easy dispersion of graphite oxide in water under mild ultrasonication. One key difference in properties between graphene and graphene oxide is that while the former is electrically conductive, the latter is insulating for the presence of saturated sp^3 bonds and electronegative oxygen atoms, as well as other "defects". The correlation between degree of oxidation and properties of the materials was extensively studied[15,16], mainly via reduction of the graphene oxide to reduce the

oxygen content and restore the sp^2 network. The material obtained, reduced graphene oxide (rGO), exhibits graphene like properties such as good electric conductivity, and can be produced in large quantities, rather rapidly and at a much lower cost than pristine graphene[17]. Furthermore, a variety of chemical[18], electrochemical[19] and thermal[20] processes can be employed for the reduction of graphene oxide. Despite many synthetic efforts though, DFT calculations have confirmed that it is impossible to completely reduce graphene oxide to graphene by chemical or thermal reduction or a combination of the two[21].

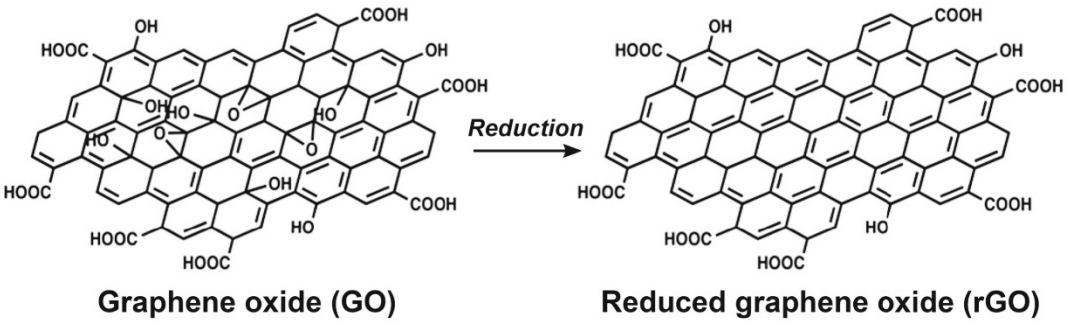

Fig. 2: Structures of graphene oxide (GO) and reduced graphene oxide (rGO).
Adapted from Tabor et al.[22]

The chemical functionalization of graphene can be achieved in a variety of other ways[23]. For example chemical doping, which consists of substituting one carbon atom with another element, is the most basic way of modifying the structure and properties of graphene, and has been employed to synthesize a wide gamut of materials. Most interesting dopants are nitrogen[24] and boron[25], since their atomic radii are very similar to that of carbon; other highly investigated dopants are S[26], P[27], Si[28] and different metals[29].

The covalent functionalization of pristine graphene via addition of free radicals or dienophiles to the sp^2 carbon atoms can be carried out, but expensive and unstable chemicals as diazonium salts must be used[30]. The presence of oxygen groups on GO can also be exploited for covalent functionalization, exploiting simple esterification

and amidation reactions, or grafting larger organic molecules such as porphyrins[31], phtalocyanines and even polymers[32]. A variety of noncovalent functionalizations of graphene and graphene oxide can be also achieved exploiting the intermolecular interactions involving the delocalized π-system of the sheets[33]. Finally, graphene sheets are also an ideal substrate for the deposition of nanoparticles and other nanostructures, due to their large active surface area, which can be even larger than graphite or carbon nanotubes. Deposition of noble metals (Pt, Au, Ag, Rh, Pd)[34], metal oxides (ZnO, TiO_2)[35] and even dichalcogenides[36] on pristine graphene or graphene derivatives produce composite materials that can be used for catalysis or optoelectronics applications[37].

2.1.3 Fluorographene

Fluorographene (fluorinated graphene, FG) can be viewed as the building block of fluorographite, which was first synthesized way back in 1934 by Ruff and Bretschneider[38]. The rise in interest in graphene brought back the attention of scientists to this material, but it wasn't until the late 2000's that FG was prepared via fluorination of graphene with XeF_2[39] and later via chemical exfoliation of fluorographite[40]. In stoichiometric fluorographene (C_1F_1) every carbon atom is sp^3 hybridized, as opposed to the sp^2 hybridation in pristine graphene, which makes FG an insulator; in addition to this, numerous studies have also shown that FG is not chemically inert, even if it contains C-F bonds, which are regarded as one of the strongest bonds in organic chemistry[41], but instead shows an electrophilic character and it can thus be used for the synthesis of tailored graphene derivatives with a high degree of functionalization.

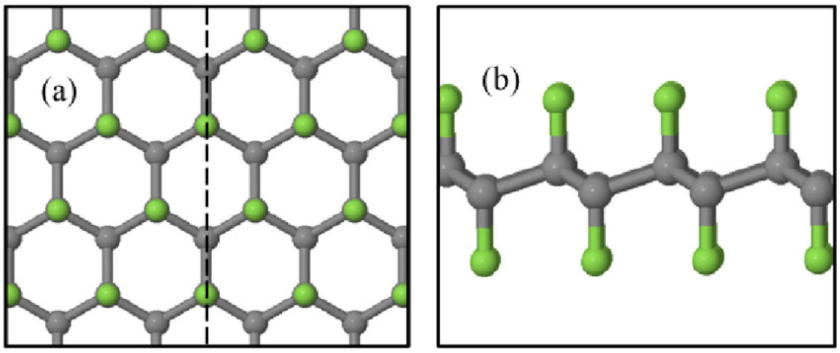

Fig. 3: a) top-down view of FG; b) side view of the chair conformation of FG.
Adapted from Yang, L.; Liang, Y.[42]

Regarding its chemical behaviour, among the many reactions that FG can undergo as an electrophile the two of most interest for this thesis are a) reductive defluorination to graphene and b) nucleophilic substitution. The former might seem unusual, given the C-F bond strength, but it is believed to be helped by the fact that the aforementioned bond in FG has a semi-ionic character according to computational data[43]; moreover, the presence of point defects in proximity of the C-F bond also favours the reaction. Defluorination to graphene can be achieved (sono)chemically and thermally, with the former found to be more effective than the latter[39], and partial defluorination is also possible. Nucleophilic substitution, on the other hand, is a bit more straight forward, and has been employed in the preparation of different covalent functionalized graphene derivatives, by reacting FG with amine- and alcohol- bearing compounds[44]. One key factor that makes these reaction particularly interesting among the other functionalization processes mentioned above, is that they proceed with rather mild conditions and relatively cleanly; for example, functionalization with acidic moieties to form graphene acid (GA) can be achieved via hydrolysis of cyanographene, obtained via substitution of FG with cyanide salts[45]. This has been a huge step in the direction of reproducible and selective functionalization of graphene with oxygen-bearing groups, since the synthesis of graphene oxide usually requires

very harsh oxidizing agents and conditions (K_2MnO_4, $NaNO_3$ and concentrated H_2SO_4 for the most commonly employed Hummers' method[46]) which profoundly affect the properties, structure and stoichiometry without selectivity[47,48].

2.1.4 Graphene Acid

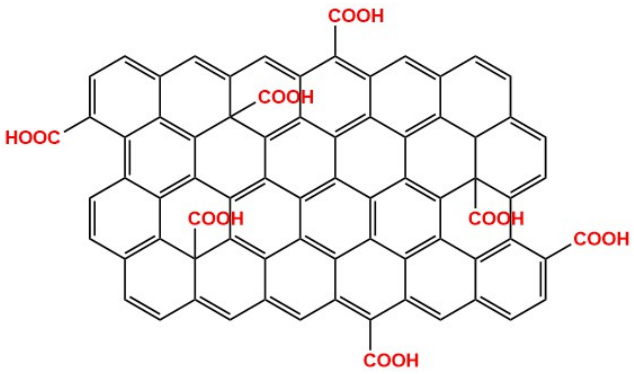

Fig. 4: Structure of graphene acid.

The term graphene acid has been assigned to different COOH-rich systems with very different properties and on prepared by many synthesis routes. Sofer et al.[49] in 2016 called GA a material obtained via multiple successive oxidations of GO to remove any other oxygen-containing functional groups. Concentrations up to 30 wt% of COOH can be obtained using this method, however the final product does not possess the typical properties of a graphene, reaching a 3D wrinkled structure because of the strong hydrogen bonds between single sheets and showing aggregates with a size of hundreds of nanometers. Furthermore, high resolution photoemission spectra show that the contribution of sp^2 carbons to the C1s peak is almost zero, making this material very different in structure from a functionalized graphene. More recently, Otyepka et al.[45] have synthesized cyanographene starting from fluorographene (Fig. 5), via reaction of exfoliated commercial fluorographite and NaCN in DMF, obtaining a functionalization degree of 15% (or 24 wt%). In the same work, cyanographene was subjected to acid hydrolysis with 20% HNO_3 yielding GA, with a functionalization degree of 13% and an estimated stoichiometry of $C_{6.6}(COOH)_1$; the

degree of functionalization was found to be greater than any covalently functionalized graphene derivatives previously reported.

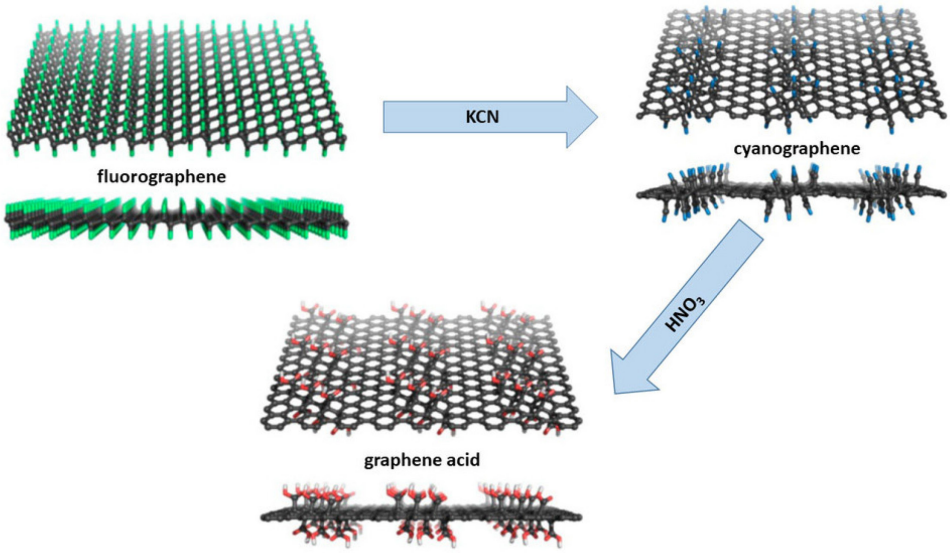

Fig. 5: Schematic of the synthetic procedure for cyanographene and GA employed by Otyepka et al.[45]; F: green; N: blue; O: red; H: white.[50]

Other than the aforementioned selectivity in its functionalization, there are some other differences between GA and GO. Firstly, the acidic moieties in GA are arranged in a very homogeneous fashion, with COOH groups present both on the basal plane and on the edges of the flakes, while in GO they are located mainly on the edges with the basal plane mainly covered in hydroxyls and epoxides according to the widely accepted Lerf-Klinowski model[51]. Furthermore, GA exhibits a very good conductivity, order of magnitudes higher than the that in GO: the sheet resistance, a measure of resistivity of thin films and thus inversely related to conductivity, is 6800 Ω sq^{-1} for GA versus 2174 $\times$ 10^6 Ω sq^{-1} for GO. Conductivity is also similar to other covalent functionalized graphene derivatives, despite the higher functionalization degree[45].

The relatively high amount of homogeneously distributed COOH groups makes GA particularly interesting for further functionalization, as explored by Otyepka and

coworkers[45] who achieved covalent binding through amide bonds using the carboxylic groups present on the basal plane. Later in the same research group GA was functionalized with ferrocene[52], exploiting a first amidation over the carboxylic groups using propylendiamine (PDA) and then a second amidation of the free dangling amine with ferrocenecarboxylic acid (Fig. 6). This surface modification allows the preparation of hybrid materials and the heterogenisation of a molecular catalyst, producing a material that combines the high selectivity of the homogeneous active species with the stability and recyclability of the heterogeneous supports. In this particular case a 3.6 at% of iron was introduced in the final material.

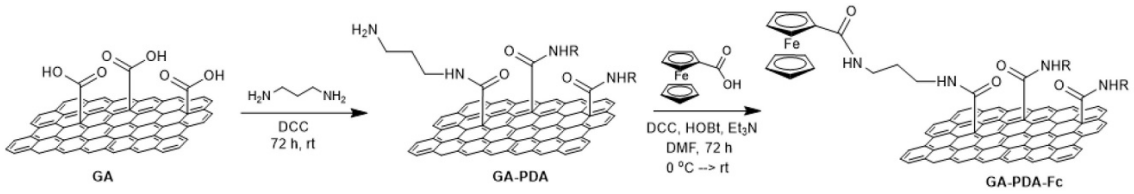

Fig. 6: Synthetic procedure for the functionalization of GA with ferrocene[52].

Not surprisingly, the same synthetic procedure carried out with GO leads to the binding of only up to 1.0 at% of iron, considerably less than the case with GA because of the selective and controlled functionalization in the latter. Both the hybrid materials were tested in the C-H insertion of diazonium salts into arenes, a reaction homogeneously catalysed by molecular ferrocene, finding that GA-based catalyst was more active than that based on GO, thanks to the more extended sp^2 domains that make easier the adsorption of the catalytic substrate near the active sites. Other similar functionalizations have been explored, such as the binding of a Co-based molecular catalyst for the visible-light driven conversion of CO_2 to CO and formate[53] and the immobilization of small Pd nanoparticles (down to 0.6 nm of size) for C-C homo and cross-coupling[54]. Furthermore, the possibility of anchoring single-atom transition metals to GA to prepare the so-called Single Atom Catalysts (SACs), in which all the

supported metal species are present as isolated atoms and thus highly dispersed and active, has been recently investigated theoretically[55]. For what concerns this work, the most interesting application of GA is surely its use as a carbocatalyst, as will be presented in the next paragraphs.

2.2 Catalytic activity of graphene derivatives

2.2.1 Carbocatalysis

Carbocatalysis is a type of catalysis that employs carbon-based materials as heterogeneous catalysts mainly in the field of organic chemistry, but also in electro- and photocatalysis. The main goal of carbocatalysis is to find and use different nanostructured materials such as carbon nanotubes, fullerenes, graphene and its derivatives to replace commonly used (transition) metal-based catalysts. The switch to carbocatalysts would be advantageous under many aspects. Firstly, they are all heterogeneous catalysts and thus can be recovered, washed and recycled fairly easily unlike metal-based catalysts, which are mostly homogeneous with few exceptions such as metallic Pd and Pt. Although heterogeneity comes at the cost of selectivity and activity, the scientific interest and research aim to narrow this performance gap through functionalization of the materials and optimization of the reaction conditions. Furthermore, carbocatalysts are generally much cheaper than metal-based catalysts, and also safer for the human health and environment: most of the carbon nanomaterials are in fact biocompatible and easier to dispose after use. A lot of research efforts have been made on synthesizing these catalysts starting from biomasses, and using them in the production of biodiesel making the entire process as “green” as possible[56]. The challenge in achieving good results in heterogeneous

metal-free catalysis arises from the fact that the chemistry of the system is profoundly dependent on the properties of the nanostructured catalyst, which are very peculiar and difficult to predict because of the size and the morphology of the materials. The mechanistic aspect of the reaction can also vary a lot with the conditions, and the intrinsic defectivity of carbon-based nanomaterials can make it difficult to identify exactly the active species involved.

The term carbocatalysis was first proposed in 2010 by Bielawski and coworkers[57] who demonstrated that GO was able to convert alcohols, alkenes and alkynes to aldehydes or ketones; however, a very high loading of GO vs substrate (200 wt%) was employed to reach good conversions, and a later investigation on the mechanism on the oxidation of benzyl alcohol to benzaldehyde[58] made clear that in that particular case GO was not a catalyst for the oxidation, but rather the oxidant itself: when used in substoichiometric amounts, up to 73% of oxygen was lost in the recovered material after the reaction. Graphene acid was also employed as a catalyst in the same reaction[59], but with a much lower catalytic load (5 wt%) and the use of HNO_3 as a cocatalyst, reaching complete conversion at 90°C in just 2 hours: this set a new standard for the carbocatalytic oxidation of benzyl alcohol with a Turn Over Frequency (TOF) of 152 mmol of substrate converted per gram of catalyst per hour, higher than other carbocatalysts and even some noble metal catalysts[50]. Moreover, the catalyst remained active for more than 10 cycles without any major modification of composition or surface structure. DFT calculations shed light on the mechanism and the role of the COOH groups in GA, whose role is to bind selectively the nitric acid and promote a series of electron transfers and redox reactions which ultimately lead to the oxidation of benzylic alcohol.

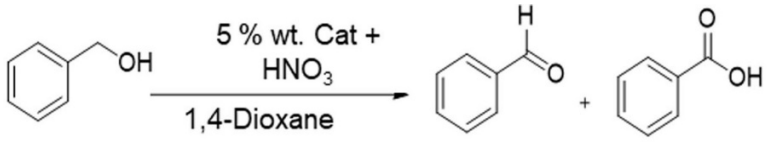

Fig. 7: Oxidation of benzylic alcohol catalyzed by GA.[50]

2.2.2 Aerobic oxidations

Aerobic oxidations aroused a great deal of interest in the last years, given that the possibility of exploiting the very abundant and harmless molecular oxygen for synthetic purposes fits right in with the green chemistry principles[2]. Coupling this with the use of carbocatalysts is a huge step forward towards sustainability of chemical syntheses and processes. Oxidation of C-H bonds is generally not an easy task, and harsh oxidants such as permanganates and dichromates are usually employed. Since benzylic C-H bonds are more reactive than alkyl ones, most of the catalytic studies are focused on the oxidation of benzylic alcohols and hydrocarbons.

Pristine non-defective graphene does not show appreciable activity in aerobic oxidations, while the presence of heteroatoms can introduce catalytic activity towards this type of reaction: for example, N-doped reduced graphene oxide (N-rGO) obtained by thermal annealing was found to be active in the selective conversion of benzyl alcohol to benzaldehyde[60], with a modest 15% maximum conversion reached during the tests; the reaction is believed to proceed via the activation of molecular oxygen through the formation of an N-O_2 sp^2 intermediate over the nitrogen dopant atoms; in fact, undoped rGO showed negligible activity. In another work by Garcia et al.[61], nitrogen (N)-, boron (B)- and boron, nitrogen (B,N)-doped graphenes were also tested as catalysts for the aerobic oxidation of benzylic positions and of styrene, reaching good conversions of the substrate; the highest obtained was in the (B,N)-doped graphene catalysed oxidation of tetralin, in which 50% of the reagent was converted

in the products in 24h at 120°C, with a high selectivity (80%) towards the desired tetralol and tetralone.

2.2.3 Oxidative homocoupling of amines

Among the aerobic oxidations achieved by carbocatalysts, oxidative homocoupling of amines to imines is particularly interesting, since imines or Schiff's bases are intermediates for the synthesis of a variety of drugs, fine chemicals and biologically active compounds[62–64]. Imines contain a double C=N bond which can undergo many different reactions such as hydrolysis back to amines, alkylation, allylation, aldolation, aridinization and cycloaddiction[65]; furthermore, imines are chiral and can be employed in highly stereoselective processes[66]. The most common synthetic route to obtain imines employs the acid-catalysed condensation of amines and carbonylic compounds such as ketones and aldehydes, with the latter strategy suffering from drawbacks such as the instability of aldehydes which rapidly tend to be oxidized in the air. The condensation reactions can also be challenging because of the presence of water, which has to be removed by dehydrating agents or via Dean-Stark apparatus to avoid hydrolysis of the imine, and the process must be carefully controlled to avoid formation of byproducts. For these reasons, the focus of research has moved to one-pot catalytic syntheses, such as oxidative coupling reactions: amines can react with themselves to give homocoupling reactions or with other amines to give heterocoupling reactions, with the oxygen being the final oxidant and the only byproducts being ammonia and water. As said before for benzylic oxidations, this process is more facile with benzylic amines, since the resulting imine and the intermediates are stabilized by resonance.

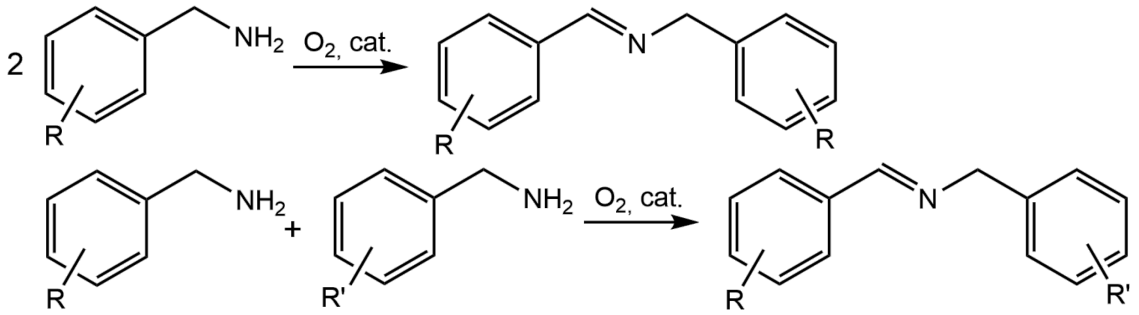

Fig. 8: Oxidative homo- (top) and heterocoupling (bottom) of benzylic amines to N-benzylidenebenzylamines.

Many metal-based catalytic systems, both homogenous and heterogeneous, have been employed for the oxidative coupling of primary amines[67], however only in the last decade or so researchers in this field have tried to switch to greener alternatives. In 2011, Liu et al.[68] found out that 4-methylbenzylamine could undergo homocoupling when in a biphasic suspension with water under O_2 atmosphere. However, the reaction proceeds at slow rates, reaching full conversion in more than a day, with selectivity towards N-benzylidenebenzylamines decreasing with increasing reaction times because of the overoxidation of the imine to oxime, amide and carboxylate salts.

The use of carbocatalysts for this reaction has also been explored. Graphite oxide obtained using modified Hummers method has been employed for the solvent-less oxidative homocoupling of benzylamine[68], with high selectivity and full conversion achieved in 4 hours, at 100°C using 50 wt% of catalyst and 5 atm of O_2. The yield of N-benzylidenebenzylamine dropped significantly when less catalyst, less pressure of oxygen or lower temperatures were used. Furthermore, the same work tested the inactivity of natural flake graphite, activated carbon, carbon nanotubes and reduced graphite oxide towards the homocoupling, underlining the importance of functionalization of graphite for activating the reaction. In 2012, Loh et al.[69] used as a catalyst for the same reaction highly porous graphene oxide generated by a sequential base and acid treatment (base-acidified graphene oxide, ba-GA) which

showed high catalytic activity yielding 98% of the product, in 12h at 90°C with a very low catalytic load (5 wt%) and using oxygen in the air as the oxidant. Interestingly, the catalytic activity showed by ba-GO is higher than GO; Loh and coworkers attributed this result to two different reasons, both explained by the proposed mechanism reported in Fig. 9: a) the base and acid treatment reduce the amount of epoxides and hydroxyls, while the carboxylic acids remain untouched; b) the base reduction generates nano-holes in the GO sheets, also generating localized spins which lay at the edges of the GO sheets where the carboxylic acids are located. The carboxylic acids anchor benzylamine and the spins activate the molecular oxygen to superoxide radical which dehydrogenates the amine, and the reaction proceeds either through benzylimine or benzaldehyde to produce N-benzylidenebenzylamine.

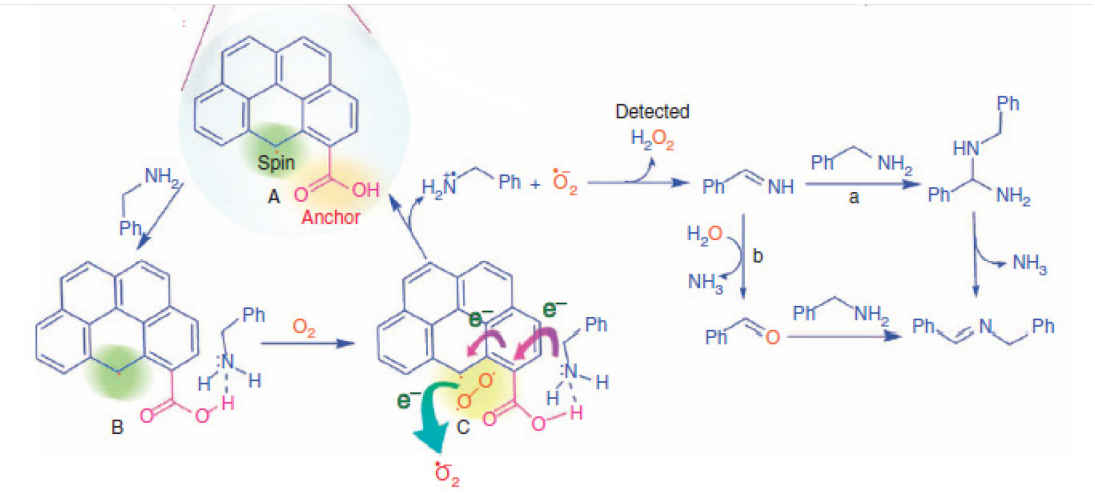

Fig. 9: Mechanism of ba-GO catalyzed oxidative coupling of primary amines.
Adapted from Loh et al. [69]

2.2.4 Oxidation of sulfides to sulfoxides and sulfones

The chemistry of organic sulfoxides and sulfones has been extensively studied in the last decades, especially for their use in pharmacology. The former in particular are used as anti-ulcer drugs and anti-acid (gastric Proton Pump Inhibitor, PPI) like omeprazole and esomeprazole, which are two of the most prescribed and consumed

drugs in the world. Sulfur atoms in sulfoxides are chiral, bearing a lone pair of electrons, which gives rise to tetrahedral electron-pair geometry and trigonal pyramidal shape: in fact, esomeprazole is just enantiopure S-omeprazole (Fig. 10). Furthermore, the rate of racemization for the stereoisomers is generally pretty low, occurring significantly only above 200°C, making sulfoxides optically stable[70].

Fig. 10: Omeprazole (left) and S-omeprazole/esomeprazole (right)

Sulfones are also found in drugs, such as the antibiotic and anti-leprotic dapsone[71], but are less commonly employed than sulfoxides. Their most important application is in polymer synthesis, with polysulfones being a class of high-performance thermoplastics[72].

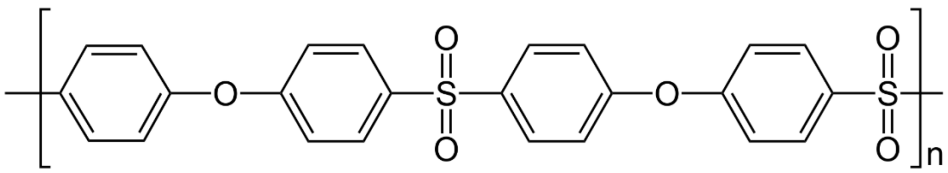

Fig. 11: An example of aromatic polysulfone, polyethersulfone (PES)

The oxidation of organic sulfides to sulfoxides and sulfones is generally carried out via transition-metal catalysis or strong oxidants[73] which are often toxic and expensive, but in the last years attention has been shifted for environmental and economic reasons to the use of the green oxidant hydrogen peroxide, due to its strength and lack of toxic by-products. In 2007, Golchoubian and Hosseinpoor[74] reported the selective conversion of a variety of sulfides to the corresponding sulfoxides in glacial acetic acid using 4 equivalents of 30% hydrogen peroxide at room temperature, with the kinetic

studies showing that the oxidation of sulfides is a second order reaction and is not acid catalyzed.

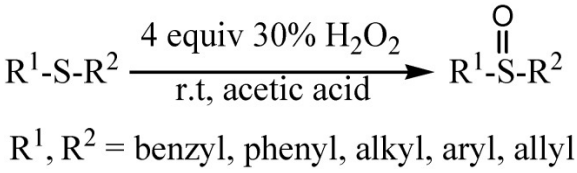

Fig. 12: Scheme of the oxidation od sulfides as reported by Golchoubian and Hosseinpoor[74].

Carbocatalysts have also been employed for this hydrogen peroxide oxidation. A highly carboxyl-decorated graphene oxide (acidic graphene oxide, AGO) prepared by oxidation of graphite with $KMnO_4$, a mixture of sulfuric and ortophosphoric acid and hydrogen peroxide[75], was tested and found selective for the oxidation of thioanisole to the corresponding sulfone[76], with full conversion achieved with 20 wt% catalytic load and 3 equivalents of H_2O_2 at room temperature in 1 hour. The mechanism proposed involves a concerted oxidation of the sulfides to sulfoxide via formation of intermediate peroxyacids (Fig. 13): the lone pairs on the sulphur atom attack the electrophilic oxygens on two adjacent peroxyacids, and the O-H bond electrons which form the double S=O bonds.

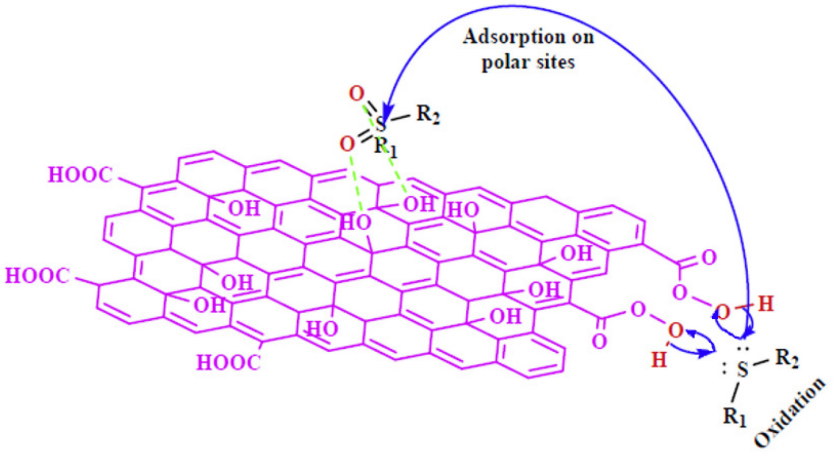

Fig. 13: Oxidation of sulfides to sulfones by AGO. Adapted from Abdi et al.[76]

The selectivity towards sulfone may be explained by the fact that carboxyilic acids in AGO are primarily located on the edges of the sheets, and this allows for the presence of two peroxyacids at the same time, reducing the possibility of mono-oxidation to sulfoxide.

3. Results and discussion

3.1 Graphene derivatives preparation and characterization

3.1.1 Graphene acetic acid (GAA)

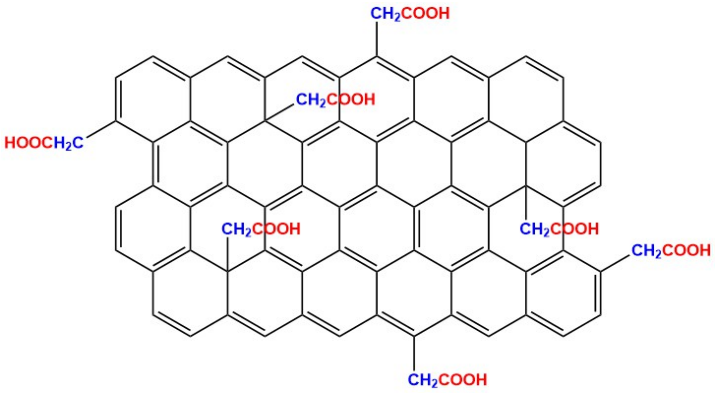

Fig. 14: Structure of graphene acetic acid (GAA).

The synthesis of graphene acetic acid was successfully accomplished in mild conditions in two steps. Given the interesting applications of graphene acid, our goal was to synthesize a graphene derivative with acid functionalization without the use of the very harmful and unsafe to handle sodium cyanide employed by Otyepka and coworkers in their synthesis[45]. The starting material was commercial stoichiometric fluorographite (C_1F_1), because of its versatility and properties reported in the introductive paragraphs. For what concerns the solvent of choice, the synthesis has been carried out in N,N-Dimethylformamide (DMF), since it is able to exfoliate fluorographite under ultrasonication and can trigger the reductive defluorination of fluorographene[77]; a working yet more expensive alternative to DMF has been found in anisole, a much more sustainable solvent as established by GSK's guide[78]. Fluorographite was suspended in the solvent (DMF or anisole) under inert conditions to avoid the presence of water in the air which could act as a nucleophile and

sonicated for 4 hours: this was enough time for fluorographite to be completely exfoliated to fluorographene (FG), but not completely defluorinated, generating sp^2 domains interrupted by sp^3 atoms still bonded to F. Separately, diethyl malonate was deprotonated by K_2CO_3 at 0°C in the solvent to form a nucleophilic carbanion, and then the two mixtures were combined and reacted under magnetic stirring at 130°C for 24 hours to allow for the substitution of the remaining fluorine atoms by the diethyl malonate. The resulting black powder was washed several times with organic solvents and water to remove any impurities (unreacted diethyl malonate, fluorides and carbonates) and then it was suspended in water and sonicated for another 4 hours. After that, the mixture was acidified to pH 1-2 and an acid hydrolysis of the esters and subsequent decarboxylation was performed at reflux for 24 hours. Once again, the resulting black powder was purified and vacuum dried.

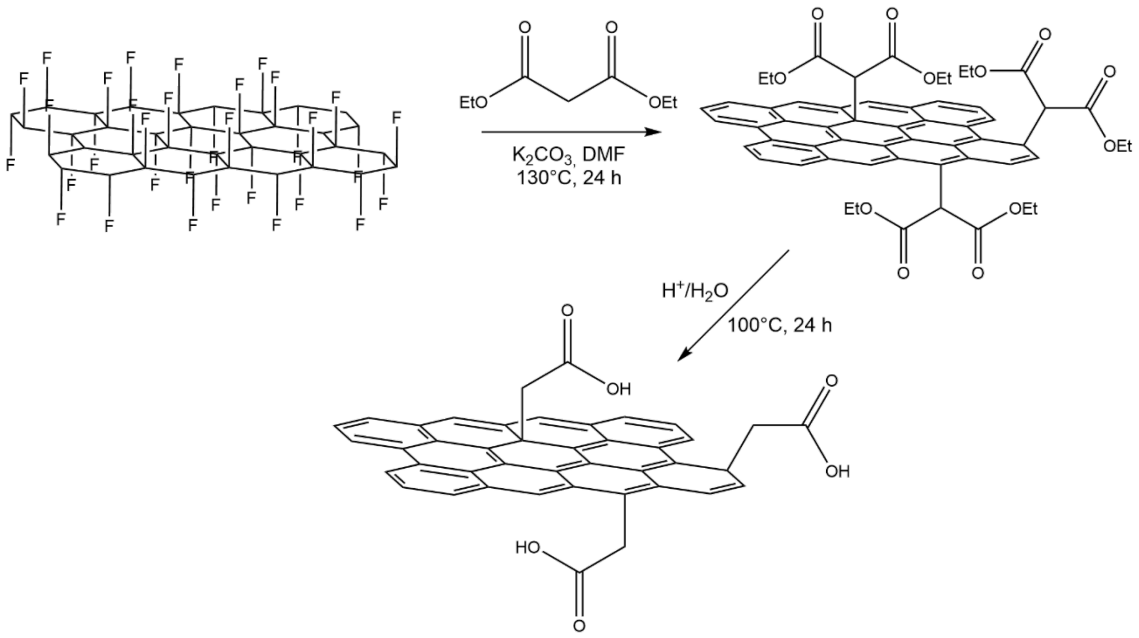

Fig. 15: Schematic of the synthesis of graphene acetic acid.

The material was characterized by several techniques. To assess its chemical composition, as well as the absence of unsubstituted fluorine, X-Ray Photoemission Spectroscopy (XPS) analysis was performed by dropcasting a thin film of the black

powder on a Cu sample holder. The sample was the introduced in a custom designed ultra-high vacuum instrumentation at pressures lower than 10^{-9} bar equipped with an electron analyser and analysed by XPS using an Al Kα photon source (see experimental section). The survey spectrum in Fig. 16 shows the presence of C and O through the respective 1s peaks, as well as Cu from the sample holder, while no fluorine is visible. Composition has been determined by normalization of the intensities of the photoemission peaks C 1s and O 1s over relative sensitivity factors, which were calculated making use of the Lindau-Yeh photoionization cross sections[79] and the inelastic mean free path obtained by the TPP-2M (Tanuma, Powell and Penn) algorithm[80]. The results of the quantification report an atomic composition of 88 at% of C and 12 at% of O. Deconvolution and fitting of the C1s spectrum allows to distinguish the different species of carbon atoms present on the material; the assignments are made according to literature[52] and are reported in Fig. 17.

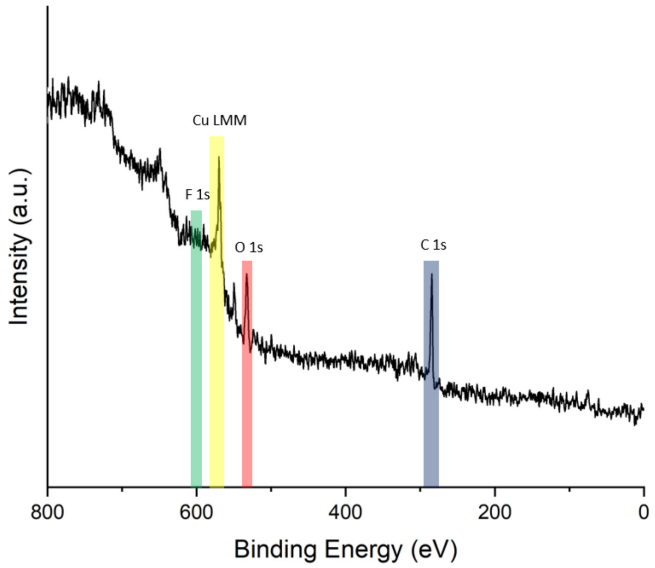

Fig. 16: XPS survey spectrum of GAA.

The analysis shows that full defluorination has been accomplished, as displayed in the survey spectrum by the lack of significant intensities at binding energies corresponding to that of F 1s as well as by the absence of any feature at around 291.0

eV in the C 1s spectrum, which is typical of C-F bonds. The fitting of the C 1s spectrum also shows that 10% of the C atoms belong to COOH functions, result comparable to that previously reported for graphene acid[45]; however the BE position assigned to the carboxyls groups is slightly lower than that reported in literature and further confirmation of the presence of such functional groups has to be obtained by other independent techniques. The remaining C-O can be derived from the presence of water in the hygroscopic potassium carbonate or in the solvent: in order to avoid this, a synthesis using degassed anhydrous solvent and an organic base has been tested, but it will not be presented in this thesis. The prevalent presence of the sp^2 domains (60% of the total C atoms, see Fig. 17) is also confirmed via C 1s spectral analysis; moreover the sp^3 peak can be both ascribed to the presence of tetrahedral C atoms where the nucleophilic substitution has occurred, as well as to the methylene bridges connecting the carboxyls pendant to the graphene sheet (blue atoms in Fig. 14).

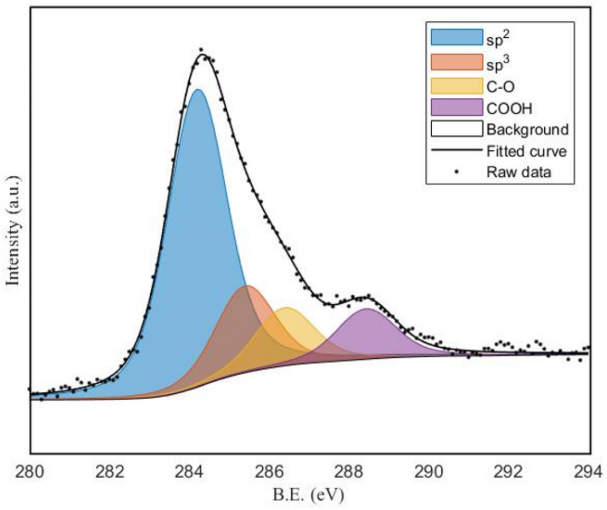

	sp^2	sp^3	C−O	O−C=O
B.E. (eV)	284.2	285.4	286.4	288.4
Amount (%)	60	18	12	10

Fig. 17: Deconvolution of C 1s photoemission peak in GAA.

Elemental analysis of the material results are reported in Tab. 1; the presence of small amounts of nitrogen can be due to solvent impurities on the material. These results differ from the ones obtained by XPS measurements but can be more accurate, since in the latter the presence of copper and copper oxides on the sample holder might affect the oxygen content. Moreover, the elemental analysis is coherent with the deconvolution of the C 1s photoemission peak.

Element	Mass %
C	70.44
O	26.41
H	2.53
N	0.62

Tab. 1: Elemental analysis of GAA.

FT-IR spectra of the material in KBr pellets were also recorded to confirm that the synthesis performed the substitution of fluorine atoms with acid functionalities. The spectrum of GAA (Fig. 18) presents 4 distinguished features: C-H stretching at around 3000 cm^{-1} (red), with the characteristic multi-peaked shape; C=O stretching at around 1730 cm^{-1} (green), aromatic C=C stretching at around 1600 cm^{-1} (blue) and C-O stretching at around 1220 cm^{-1} (yellow).

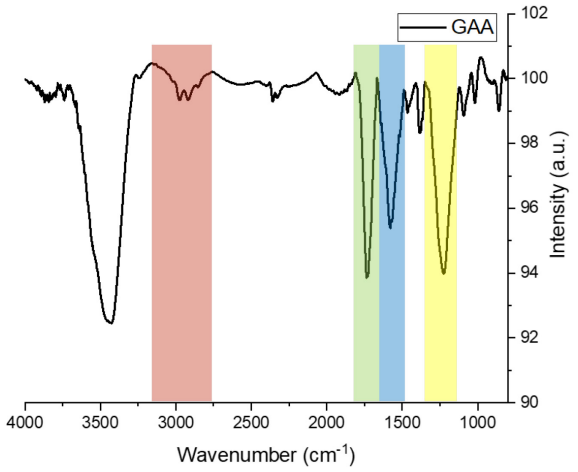

Fig. 18: Infrared spectrum of GAA. See text for colour coding.

To once more confirm the presence of carboxylic acids, the material was treated with NaOH 1M for 1h and then an IR spectrum was recorded (GAA NaOH, blue spectrum in Fig. 19); the material was then reacidified by treatment with HCl 1M and another IR spectrum was recorded (GAA HCl, black spectrum in Fig. 19). Upon base treatment, the intensity of the C=O stretching peak strongly decreases, while another peak at 1450 cm^{-1} intensifies: this latter peak is assigned to the O-C-O symmetric stretching typical of carboxylates which are formed on deprotonation of carboxylic acids. The initial situation is then restored when carboxylates are reprotonated, and this confirms that the majority of the C=O species present on the material are indeed carboxylic acids.

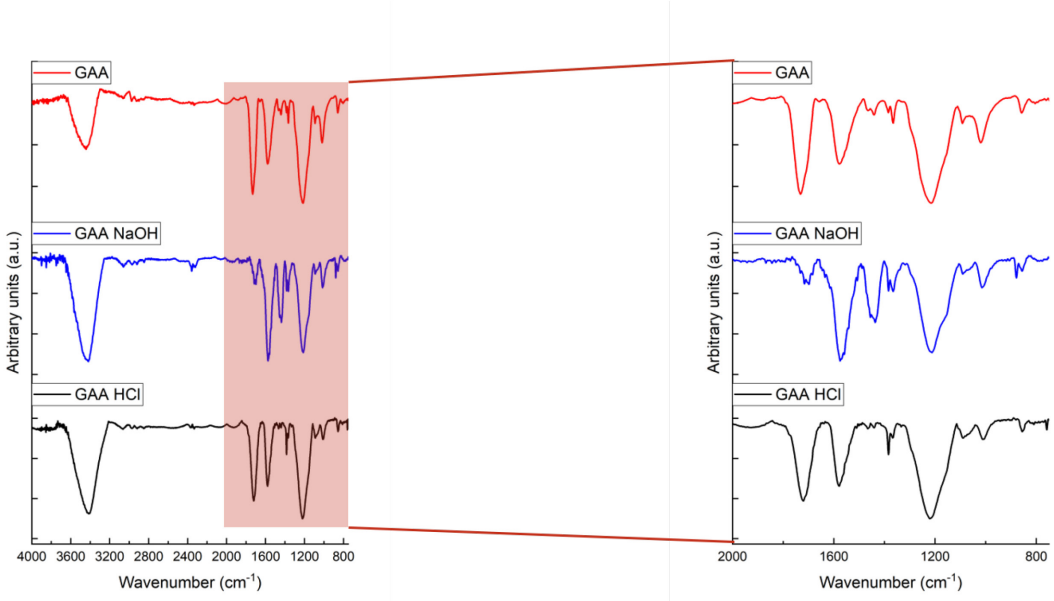

Fig. 19: Full spectra (left) and zoom (right) of GAA upon basic treatment and subsequent acid treatment.

Solid state ^{13}C NMR spectroscopy was also performed by Professors Claudio Garino and Roberto Gobetto at University of Turin. The ^{13}C spectrum acquired without any decoupling is reported in Fig. 20, with the assignment of peaks and their relative concentration reported in Tab. 2. This analysis is coherent with the fitting of the C 1s photoemission peak and confirms the 10% COOH functionalization on the material; solid state NMR also allows to distinguish the sp^3 carbon atoms present on the graphene plane, at lower chemical shift (5-20 ppm), from the methylenic carbon atoms deshielded by the presence of the carboxylic acid (30 ppm). Furthermore, decoupled spectra do not differ significantly from the non-decoupled one, which is also informative since it confirms the absence of hydrogen atoms directly bonded to carbons (see Fig. 35 in experimental section).

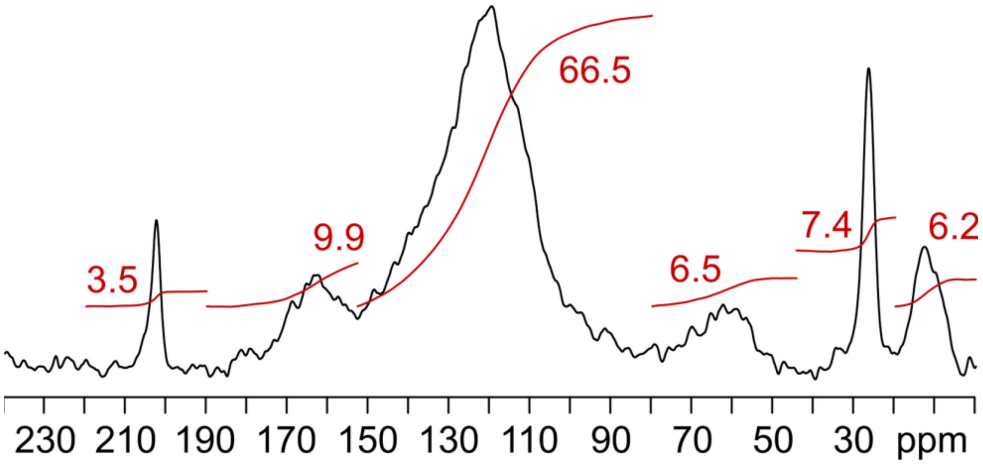

Fig. 20: ^{13}C solid state NMR of GAA.

ppm	Identification	Amount%
5-20	sp^3	6.2
30	CH_2	7.4
50-70	C-O	6.5
100-150	sp^2	66.5
150-180	COOH	9.9
210	C=O	3.5

Tab. 2: Peak assignments in ^{13}C solid state NMR of GAA.

To ultimately confirm the structure of the material and the functionalization degree, Thermal Gravimetric Analysis (TGA) has been carried out. The sample was heated at a constant rate up to 800°C under inert atmosphere while being weighed with a microbalance. The results reported in Fig. 21 show an early small loss of mass at around 130°C due to the presence of high boiling solvents like water and DMF; after that, a loss accounting for around 34.5% of the total mass is observed with the maximum of the peak at 300°C. This result is coherent with the previous elemental analysis and can be assigned to the full decarboxylation of the COOH functional groups. Unfortunately, we were unable to perform an Evolved Gas Analysis (EGA) experiment to confirm the desorption of carbon dioxide.

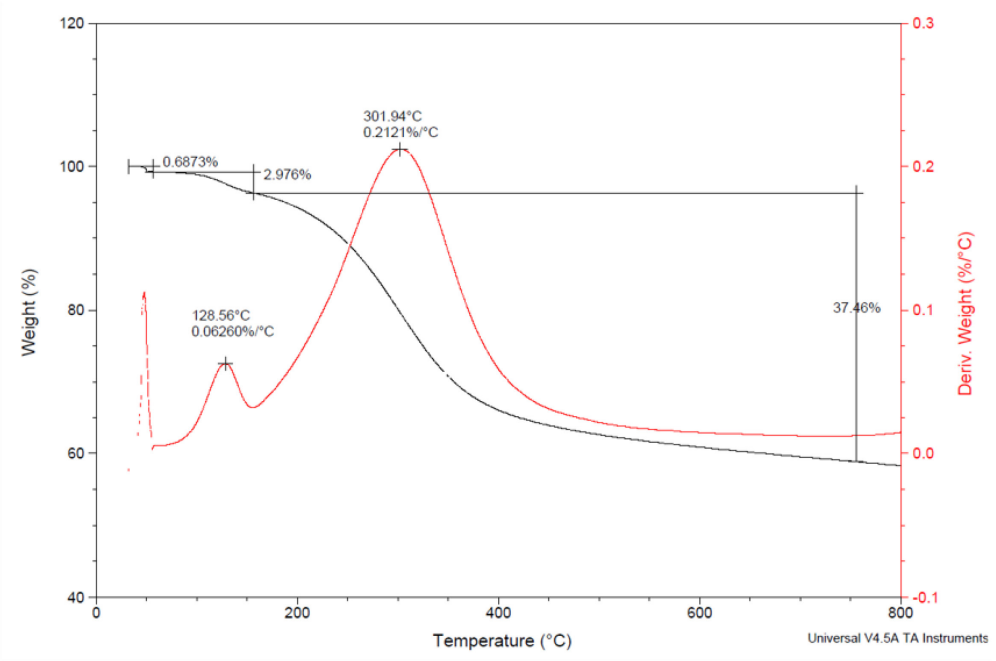

Fig. 21: Thermogravimetric analysis of GAA.

X-Ray Diffraction on GAA powder was also conducted, with the resulting diffraction pattern reported in Fig. 22. The three broad features can be ascribed to the material, and are similar to those of graphene oxide [2Θ=11.5°, (001)] and reduced graphene oxide [2Θ=24° (002) and 2Θ=47° (102)][81], confirming the presence of oxygenated functional groups in GAA, which increase the distance between layers with respect to graphite [2Θ=26.5° (002)].

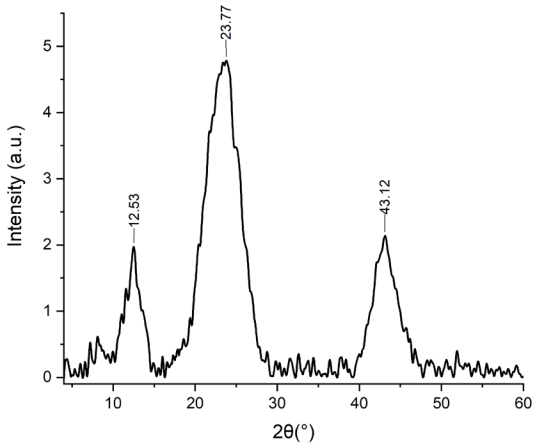

Fig. 22: X-Ray diffraction pattern of GAA.

Once established the structure of GAA, reported in Fig. 14 and Fig. 23, Z-potential measurements were performed to understand how the material behaves in water suspension. The Z-potential curve at different values of pH is reported in Fig. 23: below pH=5, the potential is approximately zero, showing that no charge is present on the surface of the material; above pH=5 Z-potential is strongly negative, because of the deprotonation of carboxylic acids. Other than to determine the surface charge, the Z-potential is better used to describe the stability of a colloidal suspension: generally, suspensions with Z-potential more positive than +30 mV and more negative than -30 mV are considered stable, and this is the case for GAA between pH 5 and 11.

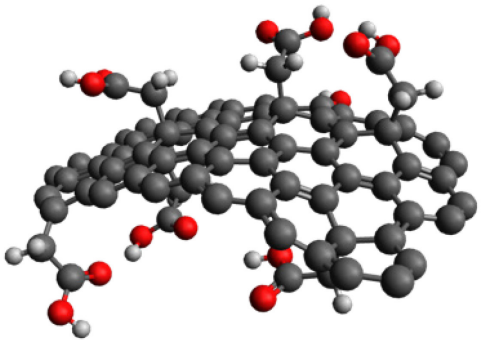

Fig. 23: Ball and stick model of GAA.

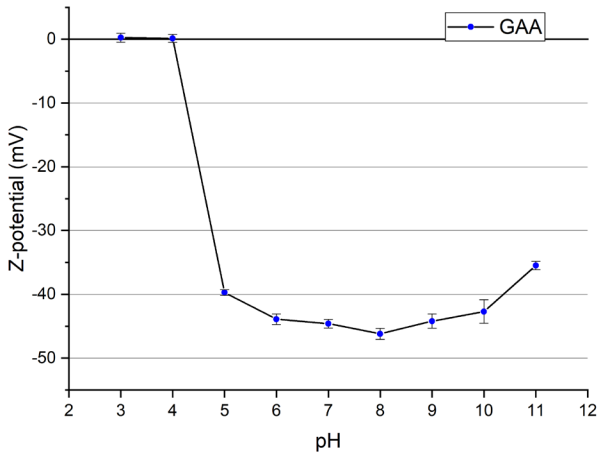

Fig. 24: GAA Z-potential curve at different pH.

Morphology of the samples was analysed by Transmission Electron Microscopy (Fig. 25). TEM images acquired show flakes of few-layer GAA, which are not planar as expected for the high functionalization degree. The flakes also show wrinkled and kinked edges, which are found also in other similarly functionalized materials.[45,52]

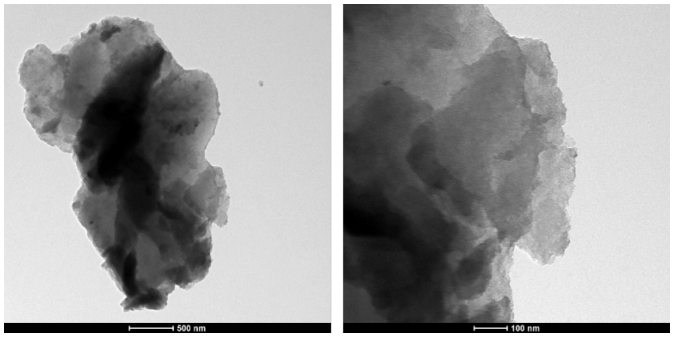

Fig. 25: TEM images of GAA.

Preliminary Electron Spin Resonance (ESR) measurement on the material were conducted by the research group of Professor Barbon in this same University. The experiments confirmed the presence of paramagnetic spins on the material, with the calculated number of spins atoms being 1 every 10^5 carbon atoms or $5.2 \cdot 10^{18}$ spin/g. This result is comparable with some other graphene derivatives: for example, rGO obtained by reduction of GO with sodium borohydride counts $6.2 \cdot 10^{18}$ spin/g[82]. The acquired experimental spectrum (Fig. 26) has been fitted with two Lorentian curves, with the lineshape showing no evident interactions of the spins with protons and ^{13}C nuclei: this means that there are efficient electron exchange processes in the material thanks to the delocalized π-system. The two components, one narrower and one broader, appear in similar materials reported in the literature: the former is generally assigned to more localized sigma dangling bonds spins, while the latter arises from spins which are to some extent delocalized along the edges of the graphene sheets[69]. These exhibit fast spin-lattice relaxation via interaction with the adjacent π-system which increases the linewidth of the peak.

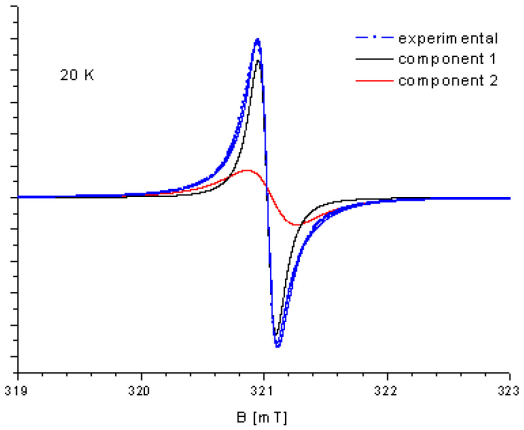

Fig. 26: ESR spectrum of GAA at 20K.

3.2 Catalytic tests

3.2.1 Aerobic oxidative homocoupling of amines

GAA was tested as carbocatalyst for the aerobic oxidation of benzylamine. We took as a reference the work of Loh and coworkers[69] and initially used the same reaction conditions to conduct the tests; the development of the reaction products was followed via ^{1}H NMR spectroscopy; the signals used to identify the species were the methylene singlets at 3.9 ppm and 4.8 ppm for benzylamine and N-benzylidenebenzylamine, respectively.

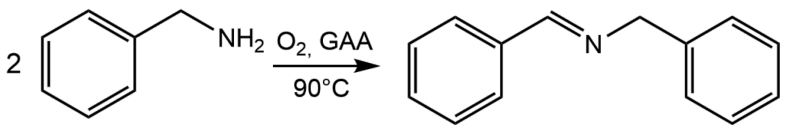

Fig. 27: Aerobic oxidative homocoupling of benzylamine catalysed by GAA.

A preliminary test was conducted in an open vial, heated at 90°C in neat of benzylamine and 10 mg of GAA (5 wt% catalytic loading) under magnetic stirring:

after 16h, no benzylamine was detected in the NMR spectrum and the only product observed was N-benzylidenebenzylamine (Fig. 28). The initial dispersion of the material in benzylamine had dried out, meaning that despite the reaction temperature was considerably lower than the boiling point of benzylamine (185°C) the reagent could evaporate. The test was repeated and to our surprise the dispersion dried just a few minutes after reaching thermal equilibrium, with only a small amount of N-benzylidene benzylamine being recovered accounting for only around 5% of the theoretical yield. To ensure that benzylamine was not irreversibly adsorbed on the catalysts, XPS experiments on the recovered GAA were conducted; however, only negligible amounts of nitrogen were found by quantitative analysis and they could not account for the loss of the reagent.

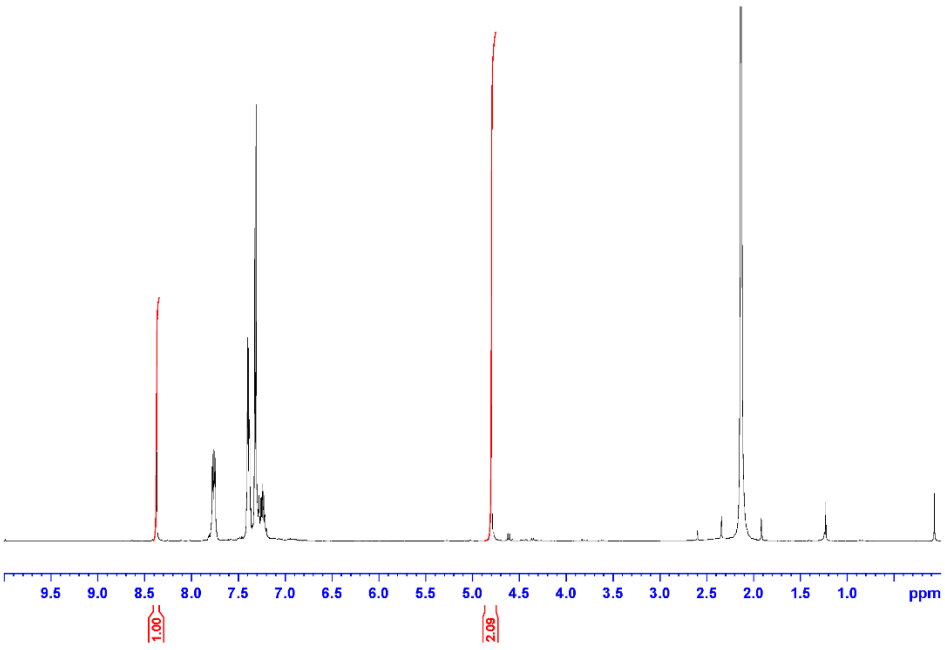

Fig. 28: NMR spectrum of the preliminary test for the aerobic homocoupling of benzylamine.

The same experiments were conducted in a 25ml round-bottom flask for 4h; at the end of the reaction the dispersion had not dried out and NMR showed the presence of both benzylamine and N-benzylidenebenzylamine. The evaporation of some of the

reagent was confirmed by the presence of a transparent liquid condensed over the colder glass walls and neck of the flask (Fig. 29), which was analysed via NMR and found to be a mixture of benzylamine and water. The latter is, with ammonia, a by-product generated by the reaction of oxidative homocoupling, and might be evaporating at 90°C removing benzylamine via stripping or formation of an azeotrope. It is noteworthy that when the reaction was conducted under N_2 atmosphere no conversion to the imine was observed, and no liquid had condensed on the walls of the flask: this confirmed that the oxygen is the final oxidant of the homocoupling reaction, and that in absence of water generated by such reaction no evaporation of benzylamine was observed.

Fig. 29: Condensation of a mixture of benzylamine and water over the cold walls of the reaction flask.

We were thus able to confirm that the material is able to activate molecular oxygen to perform benzylamine homocoupling. This did not happen at room temperature, as no N-benzylidenebenzylamine was detected even after 24h. We also found that no significant conversion was achieved below 60°C; this might confirm the presence of thermally activated paramagnetic centers on the material that transform molecular oxygen in superoxide radical and initiate the homocoupling (see mechanism reported in Fig. 9).

Despite the efforts, we were not able to avoid the loss of reagent while maintaining open air conditions; we tried covering the flask in aluminum foil to warm it evenly and using a reflux condenser, but the benzylamine-water mixture was stuck on the glass and was unable to drop back into the reaction vessel, as later found by washing the condenser and performing an NMR analysis. This unexpected behaviour of the system left us puzzled, as in the aforementioned work[69] where ba-GO was used as a catalyst Loh and coworkers were able to reach up to 98% yield of N-benzylidenebenzylamine in 12 hours, using the same open air and temperature conditions and anisole as an internal standard for GC-MS analysis.

The observed evaporation of the substrate led to other problems, such as uncertainty in determining the conversion of the reaction. To help with this, an internal standard could be used. Both 1,4-dioxane and anisole were tested, with the latter being used in the work by Loh and coworkers to determine GC-MS conversion. However, when added at the start, anisole also forms an azeotrope with water[83] and is evaporated during the reaction. This was observed when performing a kinetic test, during which aliquots were taken every hour and analysed via NMR; the yield of N-benzylidenebenzylamine calculated via internal standard method surpassed 100% after three hours and continued to increase up to 280% after six hours of reaction. Since this method is clearly faulted, we tried to plot the conversion assuming full selectivity towards N-benzylidenebenzylamine (no other by-product was detected at NMR or GC-MS) by exploiting the integrals of the methylene signals of the species using the following equation:

$$Conversion\ \% = \frac{I_{product} * 2}{(I_{reagent} + I_{product} * 2)} * 100$$

The conversion thus calculated was probably still overestimated because of the evaporation of benzylamine; however, it provided the kinetic trend reported in Fig. 30. The yield of N-benzylidenebenzylamine we obtained reached 69% after 4 hours and 86% after 6 hours.

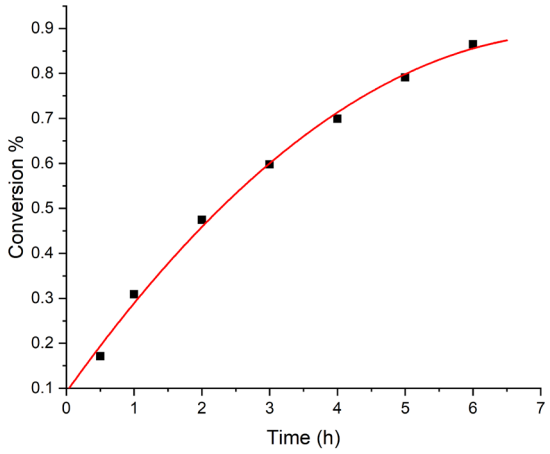

Fig. 30: Kinetic trend for the oxidation of benzylamine catalysed by GAA.

Another problem arisen with the use of anisole as internal standard was encountered when it was added at the end of the reaction directly to the mixture before separating the material, as the results obtained by this method were wildly unreliable and not reproducible. For these reasons from here to the end of the paragraph every conversion reported has been obtained via the previously used formula.

Despite the experimental issues, it seemed clear to us that the presence of the GAA was necessary to perform the oxidative homocoupling. To better understand its role in the reaction, we tried to employ as catalyst the black powder recovered after the first step of the synthesis, without it undergoing hydrolysis and decarboxylation; this material (GAA-step1) still presents most of the ester functional group derived by the diethylmalonate. In the same reaction conditions (solvent-free, open air, 4 hours, 90°C), the conversion of benzylamine was 18%, much lower than the 69% reported

for the hydrolysed GAA; this test proves the role of carboxylic acids in anchoring the amines to the material to favour the reaction with the superoxide radical (Fig. 9).

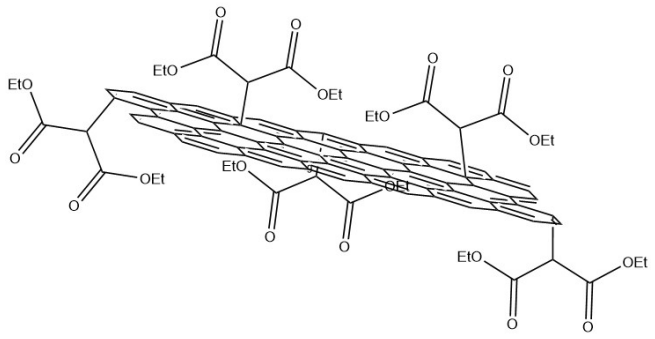

Fig. 31: GAA before undergoing acid hydrolysis (GAA-step1).

The tests have also been carried out with other primary amines available; the results obtained via NMR analysis of the reaction mixtures are reported in Tab. 3. In almost all cases evaporation of the reagent was observed, thus the influence from substituents in activating or deactivating the reaction has not been investigated. It is worth noting that in the case of the phenylethylamine the reaction proceeds really slowly as α-hydrogens in alkyl amines exhibit much lower reactivity and are not easily extracted by the superoxide; moreover, this has been the only case in which no evaporation of the reagent occurred and the conversion obtained using the internal standard matched the one calculated via the aforementioned formula.

Substrate	Product	Conversion %
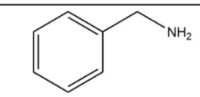	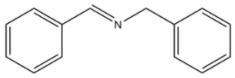	69
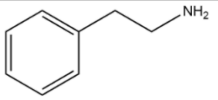	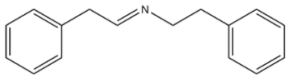	4
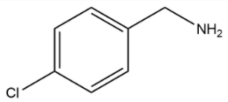	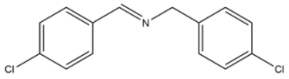	70
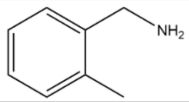	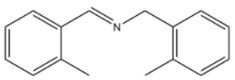	50
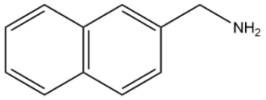	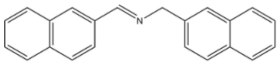	43

Tab. 3: Oxidative homocoupling of various benzylamines. All the tests have been conducted in solvent-free, open air conditions at 90°C and with a 5 wt% catalytic load of GAA.

3.2.2. Oxidation of thioanisole to methylphenyl sulfoxide

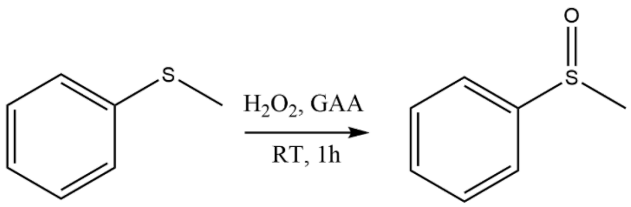

Fig. 32: Oxidation of thioanisole to methylphenyl sulfoxide catalysed by GAA.

GAA was tested as a catalyst for another reaction, the oxidation of thioanisole (methylphenyl sulfide) to the corresponding sulfoxide and sulfone. The reaction was followed via ^{1}H NMR; the signals used to determine the conversion of the substrate were the methyl singlets at 2.51 ppm, 2.78 ppm and 3.08 for the sulfide, sulfoxide and sulfone respectively. We took as a reference the work of Abdi and coworkers[76] who used acidic graphene oxide (AGO) as a catalyst for the same reaction, obtaining a very high selectivity towards the sulfone.

The reaction was conducted in a Teflon-capped vial, at 25°C, with 0.117 mL of thioanisole, 20 mg of GAA and 0.3 mL of H_2O_2 30% solution (3 equivalents) for 1h.

At the end, no reagent was detected in the NMR spectrum and the prevalent species present was the sulfoxide (Fig. 33), with a very small amount of sulfone formed. The full conversion to sulfoxide was quite unexpected, since it meant that the reactivity of GAA was completely opposite to that of AGO. We also let the reaction run for 24 hours without obtaining any significant increase in the amount of sulfone present. To shed light on the role of the species taking part in the oxidation, we tried to modify the reaction conditions (Tab. 4).

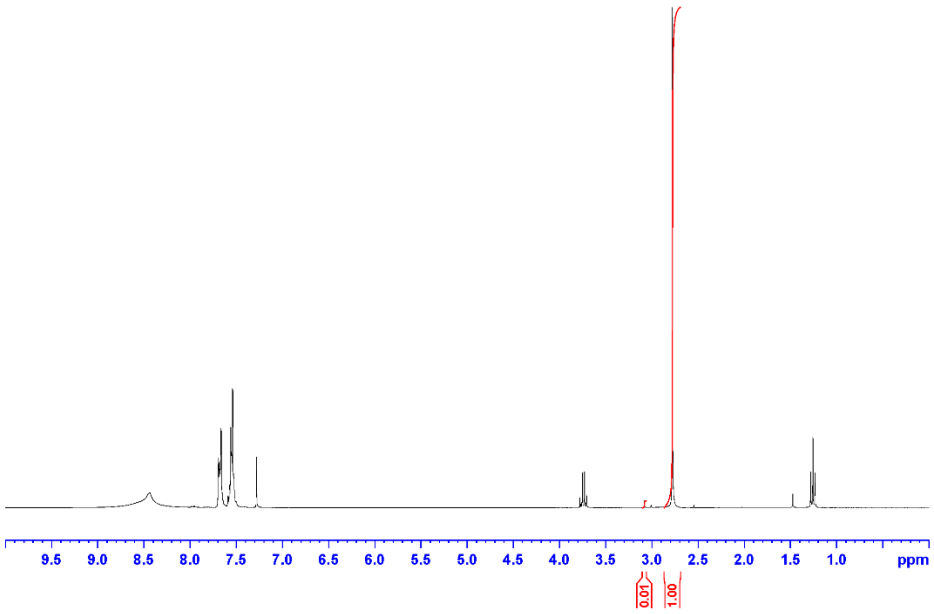

Fig. 33: NMR spectrum of the products of the oxidation of thioanisole.

The reaction without the catalyst proceeded at a lower rate, reaching only 50% conversion in 1 hour with complete selectivity to sulfoxide, underlining the efficacy of the material in speeding up the kinetics. The role of the hydrogen peroxide was also explored: when replaced with pure water no reaction occurred; when 0.1 mL of 30% H_2O_2 (1 equivalent) was used the reaction reached 60% conversion in 1 hour. Since the material is seemingly able to thermally activate oxygen as explored in the aerobic homocoupling of amines, the reaction was also conducted at 60°C in open air without the use of H_2O_2, but no conversion was detected in this case. Finally, a test

was performed in N_2 atmosphere with 0.3 mL of H_2O_2 and full conversion was once again obtained, confirming that hydrogen peroxide is the final oxidant of the reaction.

Time (h)	Cat. Load	Sulfide:H_2O_2	Conversion (%)	Sulfoxide (%)	Sulfone (%)
1	20%	1:3	99	99	1
1	-	1:3	50	>99	-
1	20%	1:1	60	>99	-
1	20%	1:0	10[a]	>99	-
1	20%	1:0	- [b]	-	-
1	20%	1:3	99[c]	>99	-
1	20%	1:3	99[d]	90	9

Tab. 4: Thioanisole oxidation tests at different conditions; where not otherwise stated, tests were conducted in a closed vial at room temperature. (a) H_2O_2 replaced by water; (b) In neat of thioanisole at 60°C, open air; (c) N_2 atmosphere; (d) after 5 cycles.

To ensure that the material is performing catalytic activity and it is not being reduced during the reaction, recycle tests were performed by simply washing the recovered GAA with ethanol and water and using it for the next run. The results showed no loss in activity or change in selectivity after 5 cycles (Fig. 34). Furthermore, XPS data on the material recovered after the 5 cycles confirms that no change in composition has occurred.

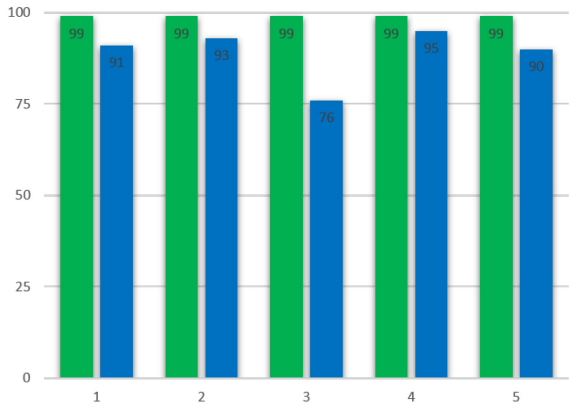

Fig. 34: Recycling tests for the oxidation of thioanisole. Conversion % (green); Selectivity % towards methylphenylsulfoxide (blue).

Further kinetic tests and a scope of the substrate should be carried out in order to identify the oxidation mechanism involving the material as catalyst. It has to be noted that the selectivity we observed using GAA is the same as the one observed by Golchoubian and Hosseinpoor in their oxidation of various sulfides using hydrogen peroxide and acetic acid[74]; for this reason we can assume that the acetic acid functionalization is somehow responsible for the oxidation of thioanisole. Taking as reference the mechanism proposed by Abdi et. al for AGO[76] (Fig. 13), we can imagine that the oxidation goes through the formation of an intermediate peroxyacid on GAA. In this case however, not all the acidic functions are located on the edges but rather homogeneously distributed over the graphene sheets; moreover, alkyl peracids are in general less reactive than benzyl peracids. These two reasons could make the concerted double oxidation of sulfides to sulfones proposed for AGO less probable when GAA is employed as a catalyst.

4. Experimental section

4.1 Syntheses and catalytic tests.

4.1.1 Synthesis of Graphene Acetic Acid (GAA)

Step 1. In a 250 mL three-necked round bottom flask, 333 mg of fluorinated graphite (FG) were suspended in 50 mL of N,N-dimethylformamide (DMF) under N_2 atmosphere and exfoliated via ultrasonication for 4 hours at room temperature. A mixture containing 26.6 g of K_2CO_3, 13.3 mL of diethyl malonate and 50 mL of DMF was stirred for 0.5 hours in an ice bath at 0°C. After the 4 hours of FG sonication, the deprotonated diethyl malonate mixture was added to the round bottom flask, and everything was heated at 130°C for 24 hours under magnetic stirring. At the end, the reaction mixture was allowed to naturally cool down to room temperature and was vacuum filtered over a polytetrafluoroethylene membrane (PTFE, 0.2 µm pore size); the recovered black powder was extensively washed with different solvents (1x100 ml of DMF and 3x100 mL of acetone over PTFE membrane, 3x100 mL of water over polycarbonate membrane) to remove any excess K_2CO_3, fluoride salts and other organic side products.

Step 2. The previously recovered black powder was dispersed in 100 mL of milli-Q water in a 250 mL round bottom flask and ultrasonicated for 4 hours at room temperature. After that, 98% sulphuric acid was added dropwise until pH of the dispersion was around 1-2. The dispersion was refluxed for 24 hours at 100°C. At the end, the reaction mixture was allowed to naturally cool down to room temperature and was vacuum filtered over a polycarbonate membrane (PC, 0.2 µm pore size); the recovered Graphene Aceto-Acid was washed with water (3x100 mL) over PC membrane and with acetone (3x100 mL) over PTFE membrane. Finally, the GAA was

dispersed in a minimal amount of acetone and vacuum dried via rotary evaporator. This process consistently yielded around 200 mg of dry, impurities free GAA.

4.1.2 Base and acid treatment of GAA

10 mg of GAA were suspended in 10 mL of NaOH 1M solution and sonicated for 1h at room temperature. The material was then filtered (but not washed) over PC membrane to obtain GAA-NaOH. This was then suspended in 10 mL of HCl 1M solution and sonicated for 1h at room temperature. It was then filtered (but not washed) over PC membrane to obtain GAA-HCl.

4.1.3 General procedure for amine homocoupling

10 mg of GAA were added to 200 mg of amine in either a 25 mL round bottom flask or a 20 mL vial and the dispersion was sonicated for 10 minutes. After that, the reaction mixture was heated at the desired temperature for the desired time (see text) under magnetic stirring. At the end, it was allowed to cool to room temperature and 10 mL of CH_3CN were added. After 10 minutes of sonication, the solution containing unreacted amine and reaction product(s) was separated via centrifugation and the solvent evaporated. Conversion and selectivity were measured on the crude reaction mixture thus obtained via ^1H NMR in $CDCl_3$. The recovered GAA was washed with acetone (3x50 mL) over PTFE membrane and with water (3x50 mL) over PC membrane and vacuum dried.

4.1.4 General procedure for the oxidation of thioanisole

20 mg of GAA were dispersed in 0.3 mL H_2O_2 30% and sonicated for 10 minutes. Afterwards, 1 mmol of thioanisole (117 µL) was added and the mixture was magnetically stirred at room temperature for 60 minutes. At the end, 10 mL of ethanol were added to the reaction mixture and sonicated for 10 minutes. The solution containing unreacted thioanisole and reaction product(s) was separated via centrifugation and the solvent removed via rotary evaporator. Conversion and selectivity were measured on the crude reaction mixture via ^1H NMR in $CDCl_3$. The recovered GAA was washed with ethanol/water mixture (1:1, 3x50mL) over PC membrane and acetone (3x50mL) over PTFE membrane, and vacuum dried before every recycling experiment.

4.2 Physicochemical characterizations

The surface chemical characterization of the materials has been carried out using X-ray photoelectron spectroscopy (XPS) in a custom-made UHV system working at a base pressure of 10^{-9} mbar, equipped with an Omicron EA125 electron analyser and an Omicron DAR 400 X-ray source with a dual Al-Mg anode. Core level photoemission spectra (C 1s, N 1s, O 1s, F 1s) were collected at room temperature with a non-monochromated Al Kα X-ray source (1486.7 eV) and using an energy step of 0.1 eV, 0.5 s of integration time, and 20 eV of pass energy. The samples were suspended in 2-propanol and drop casted on a Cu sample holder. Solid state Fourier Transformed Infrared (FT-IR) spectra were recorded on a JASCO FT/IR-4100 spectrometer by dispersing the material in KBr. Transmission Electron Microscopy images were acquired using a FEI Tecnai 12 transmission electron microscope. XRD

measurement were acquired using a Bruker D8 Advance instrument with a Cu Kα X-Ray source (0.15406 nm) at 40 kV and 40 mA. Z-potential measurements were acquired on Malvern Panalytical Zetasizer Nano ZS90 instrument using 0.3 mg/mL suspensions of GAA in water. The pH was tuned between 3 and 11 using NaOH, HCl and NaCl to maintain constant ionic strength. ^{1}H NMR spectra were acquired in $CDCl_3$ using a Bruker Avance spectrometer operating at 300 MHz and analysed with the Topspin software. We gratefully acknowledge Professors Claudio Garino and Roberto Gobetto from University of Turin for their work on the solid state ^{13}C NMR spectroscopy and Professor Antonio Barbon from this University for his work on ESR spectroscopy.

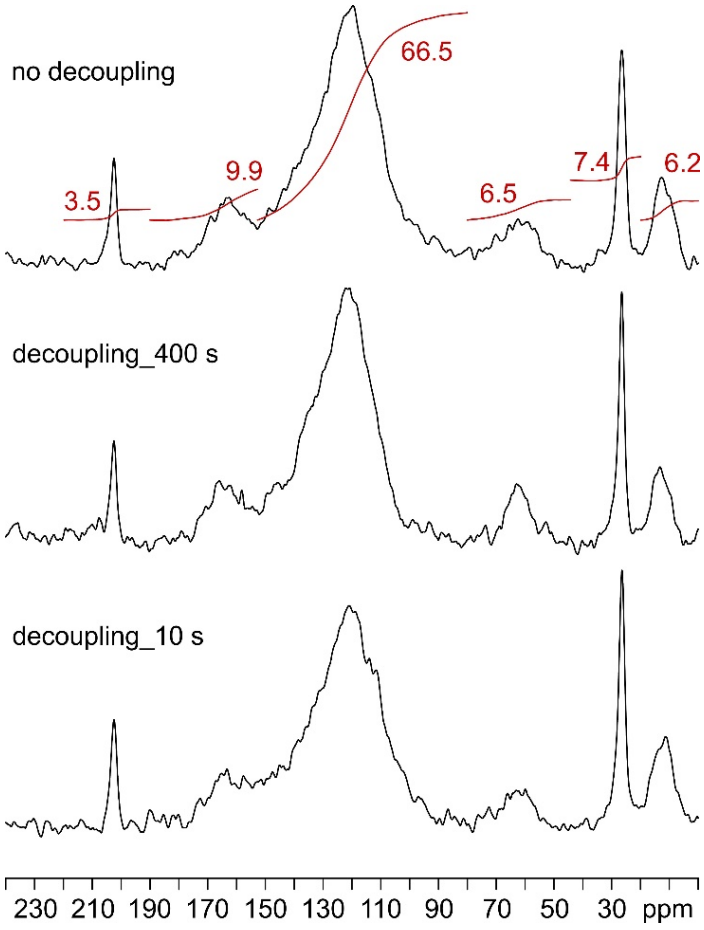

Fig. 35: Solid state NMR of GAA with decoupling.

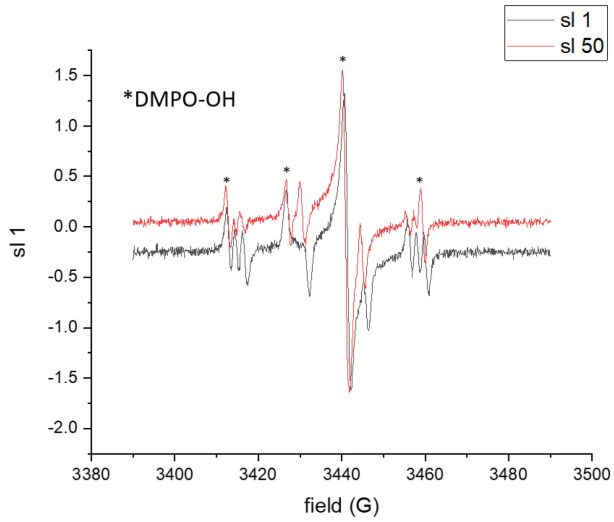

Fig. 36: EPR of spin trapping experiment on the benzylamine homocoupling system.

4.3 Reagents

4.2.1 Table of reagents

Name	Formula	MW	Hazard statements	Supplier
fluorographite	$(CF)_n$	variable	H315, H319, H335	Sigma-Aldrich
diethyl malonate	$CH_2(COOC_2H_5)_2$	160.17	-	Sigma-Aldrich
potassium carbonate	K_2CO_3	138.21	H315, H319, H335	Sigma-Aldrich
sulfuric acid, 98%	H_2SO_4	98.08	H290, H314	Sigma-Aldrich
sodium hydroxide	NaOH	40.00	H290, H314	Sigma-Aldrich
hydrochloric acid, 37%	HCl	36.46	H290, H314, H335	Sigma-Aldrich
sodium chloride	NaCl	58.44	-	Sigma-Aldrich
anisole	$CH_3OC_6H_5$	108.14	H226, H336	Sigma-Aldrich
benzylamine	$C_6H_5CH_2NH_2$	107.15	H302 + H312, H314	Sigma-Aldrich

2-phenylethylamine	$C_8H_{11}N$	121.18	H290, H301, H314	Sigma-Aldrich
4-chlorobenzylamine	$ClC_6H_4CH_2NH_2$	141.60	H302 + H312, H314	Sigma-Aldrich
2-methylbenzylamine	$CH_3C_6H_4CH_2NH_2$	121.18	H314	Sigma-Aldrich
2-naphtylmethylamine	$C_{11}H_{11}N$	157.21		Sigma-Aldrich
thioanisole	$C_6H_5SCH_3$	124.20	H302, H315, H317, H411	Sigma-Aldrich
hydrogen peroxyde, 30%	H_2O_2	34.01	H318	Sigma-Aldrich
N,N-dimethylformamide	$HCON(CH_3)_2$	73.09	H226, H312 + H332, H319, H360D	Sigma-Aldrich
acetone	$(CH_3)_2CO$	58.08	H225, H319, H336	Sigma-Aldrich
ethanol	CH_3CH_2OH	46.07	H225, H319	Sigma-Aldrich
2-propanol	$(CH_3)_2CHOH$	60.010	H225, H319, H336	Sigma-Aldrich
acetonitrile	CH_3CN	41.05	H225, H3012 + H312 + H332, H319	Sigma-Aldrich
chloroform-d	$CDCl_3$	120.38	H302, H315, H319, H331, H336, H351, H361d, H372	Sigma-Aldrich

4.2.1 Compounds spectra

The following ^{1}H NMR spectra in $CDCl_3$ were either recorded by us or were reported in the literature.

Benzylamine: 1.45 ppm (2H, s); 3.84 ppm (2H, s); 7.3 ppm (5H, m)

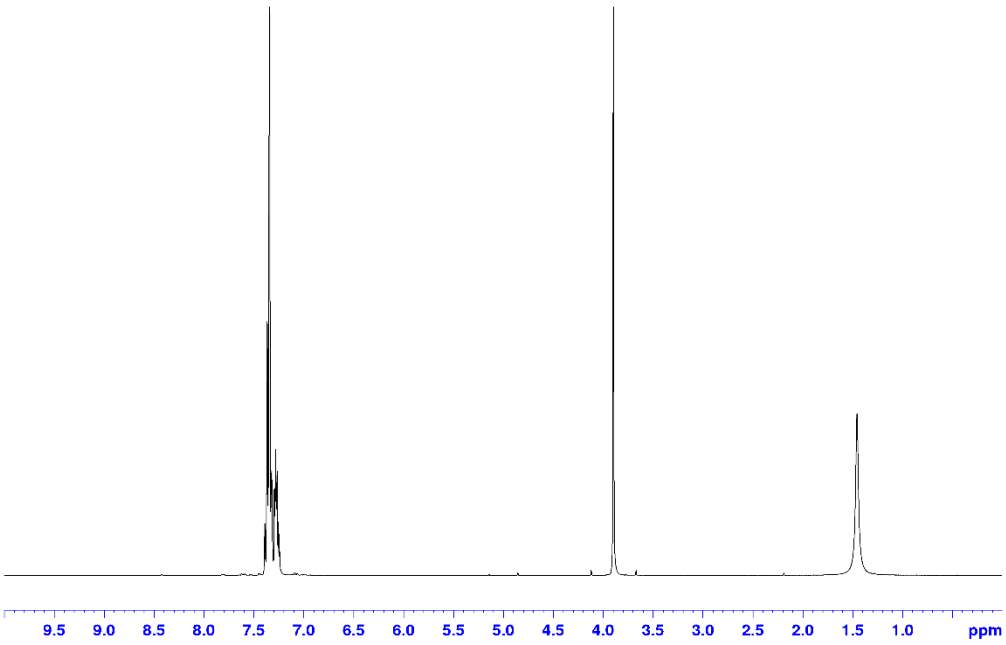

N-benzylidene benzylamine: 4.8 ppm (2H, s); 7.1-7.9 (10H, m); 8.32 ppm (1H, s)

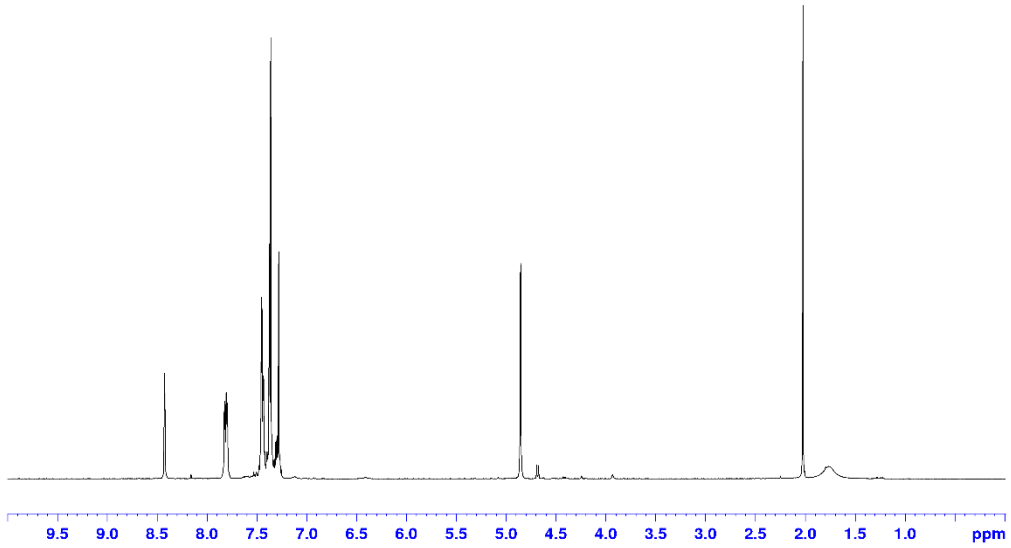

2-Phenethylamine: 1.1 ppm (2H, s); 2.7 ppm (2H, t); 2.9 ppm (2H, t); 7.1-7,4 (5H, m)

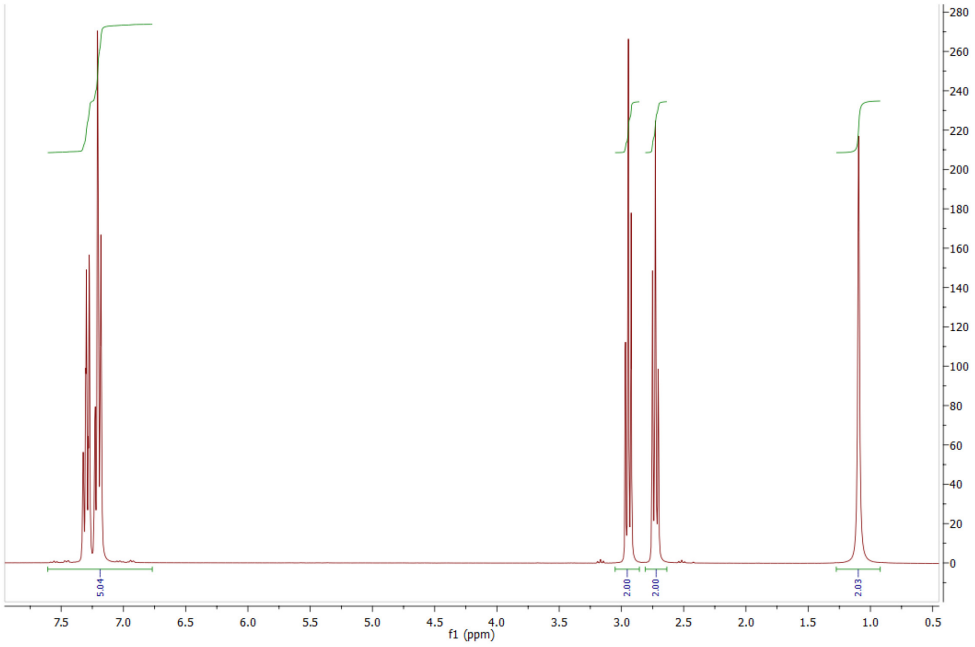

N-phenethyl-2-phenylethan-1-imine: 3.02 ppm (4H, m); 3.85 ppm (2H, t); 7.1-7.9 (10H, m); 8.2 (1H, s)

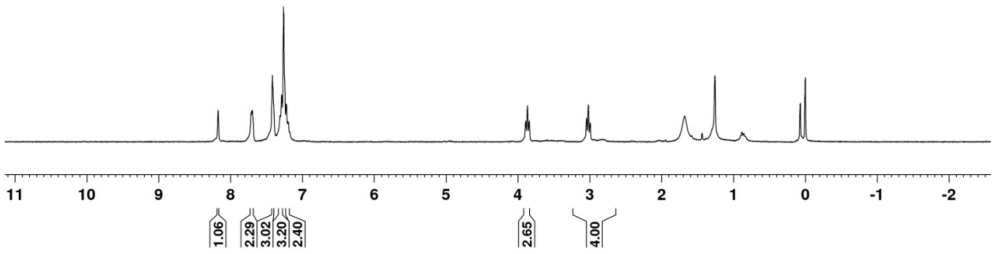

4-chlorobenzylamine: δ(ppm): 7.50 (d, 2H), 7.12 (d, 2H), 6.55 (brs, 2H), 4.80 (s, 2H)

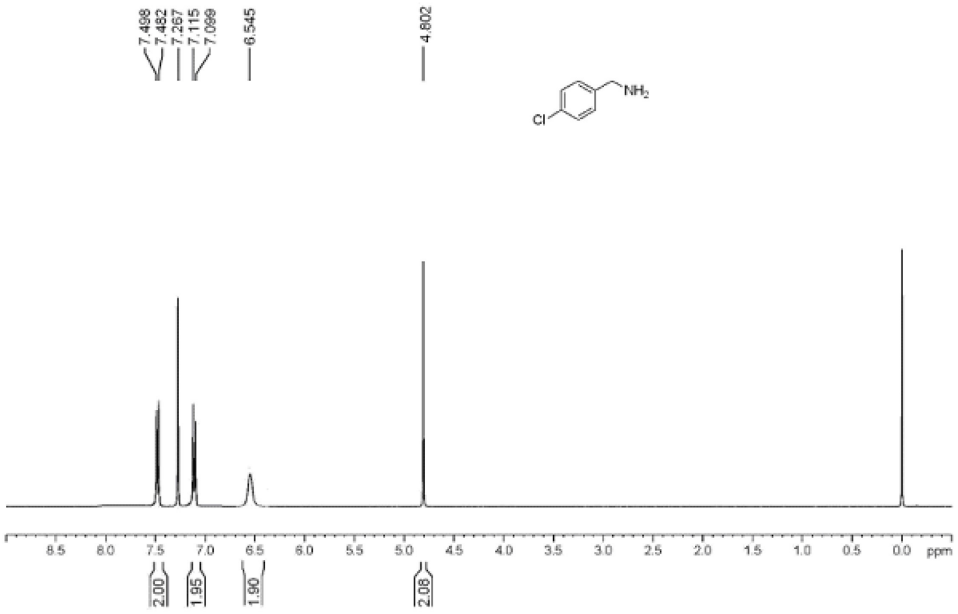

N-(4-chlorobenzylidene) 4-chlorobenzylamine: δ (ppm): 8.34 (s, 1H), 7.71 (d, 2H), 7.40 (d, 2H), 7.33-7.27 (m, 4H), 4.77 (s, 2H)

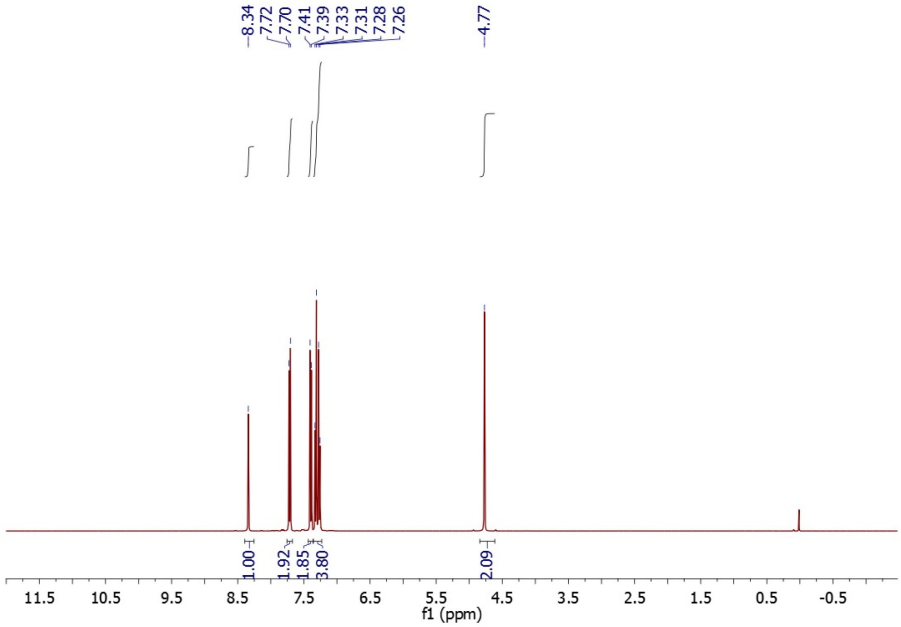

2-methylbenzylamine: δ (ppm): 7.29-7.14 (m, 4H); 3.83 (s, 2H); 2.32 (s, 3H); 1.48 (brs, 2H)

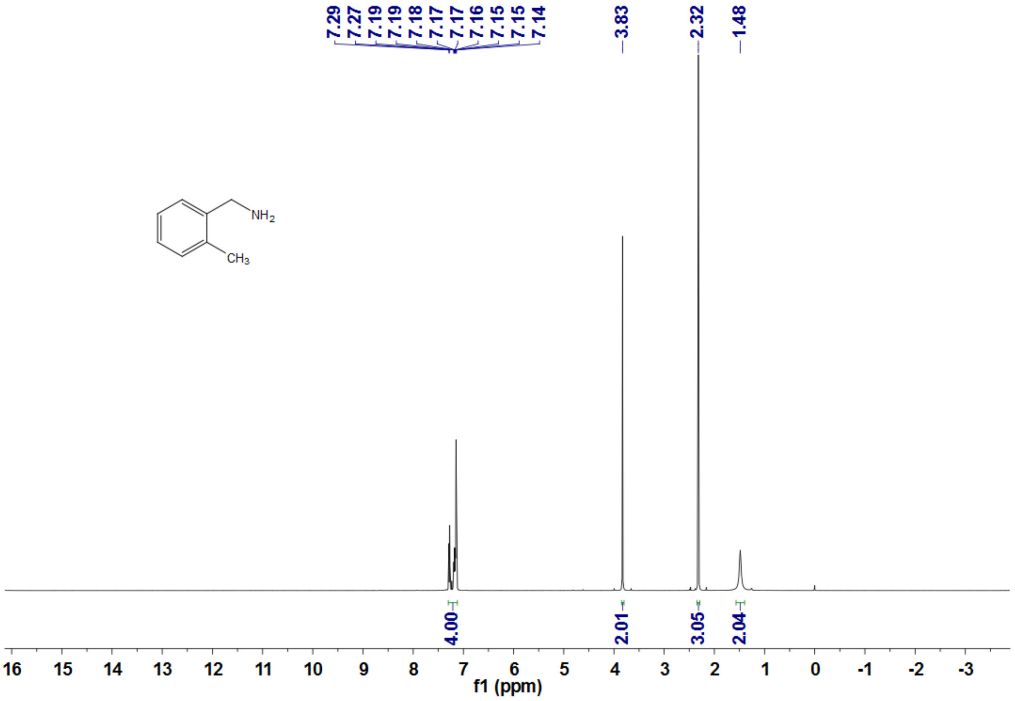

N-(2-methylbenzylidene) 2-methylphenylmethylamine: δ (ppm): 8.66 (s, 1H), 7.92 (d, 1H), 7.30-7.27 (m, 2H), 7.24-7.21 (m, 1H), 7.18-7.16 (m, 4H), 4.82 (s, 2H), 2.49 (s, 3H), 2.38 (s, 3H)

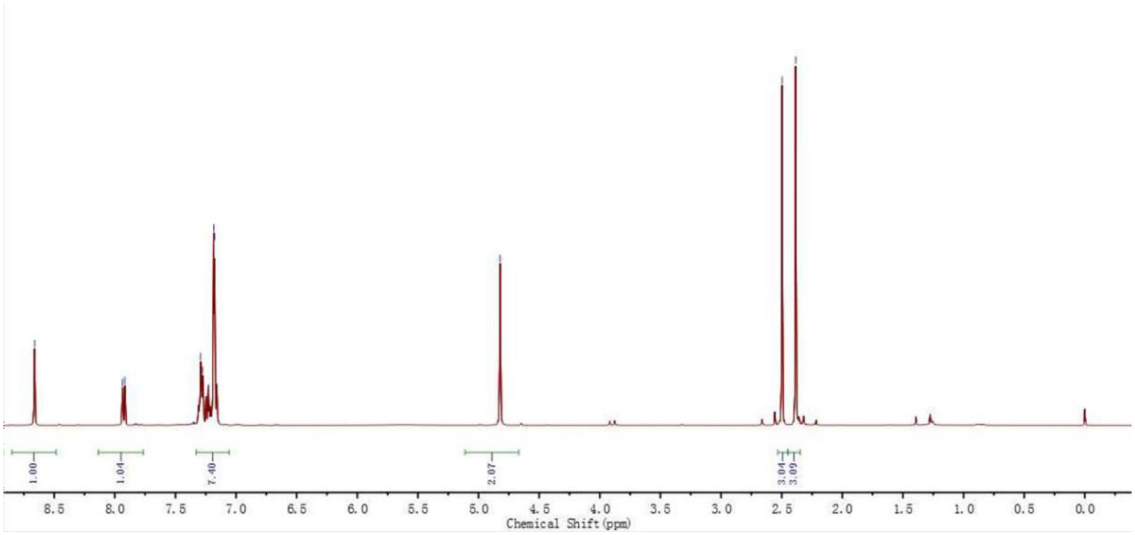

2-naphtylmethylamine: δ (ppm): 7.82 (m, 4H), 7.39-7.51 (m, 3H), 4.03 (s, 2H), 1.56 (s, 2H)

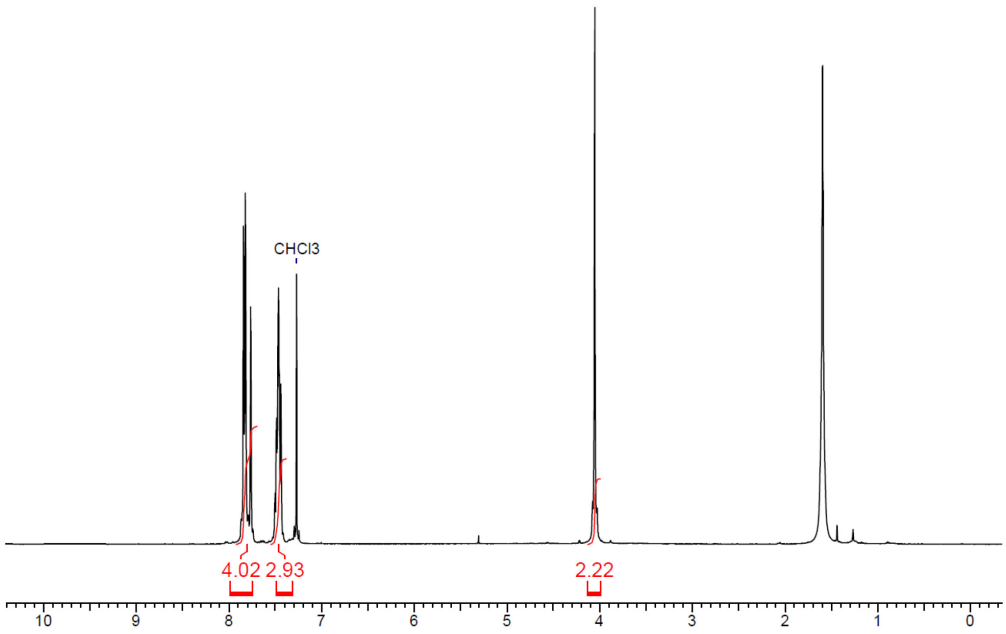

N-naphthylidene(2-naphthalene)methylamine: δ (ppm): 5.05 (s, 2H), 7.43-8.10 (m, 14H), 8.61 (s, 1H)

Thioanisole: δ (ppm): 7.32 – 7.20 (m, 4H), 7.17 – 7.07 (m, 1H), 2.47 (s, 3H)

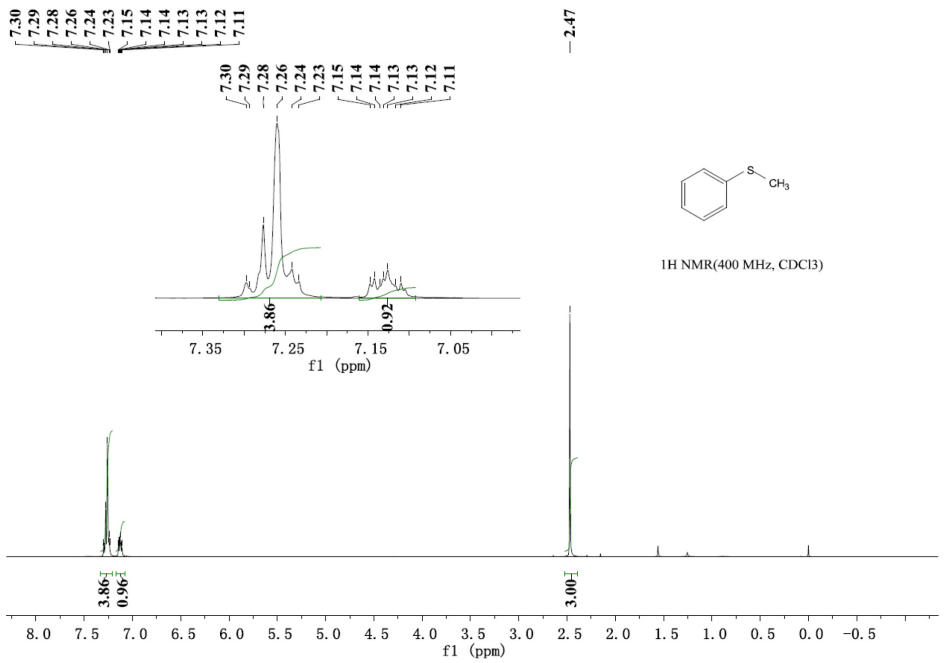

Methylphenyl sulfoxide: δ (ppm): 7.62-7.60 (m, 2H), 7.51-7.44 (m, 3H), 2.68 (s, 3H)

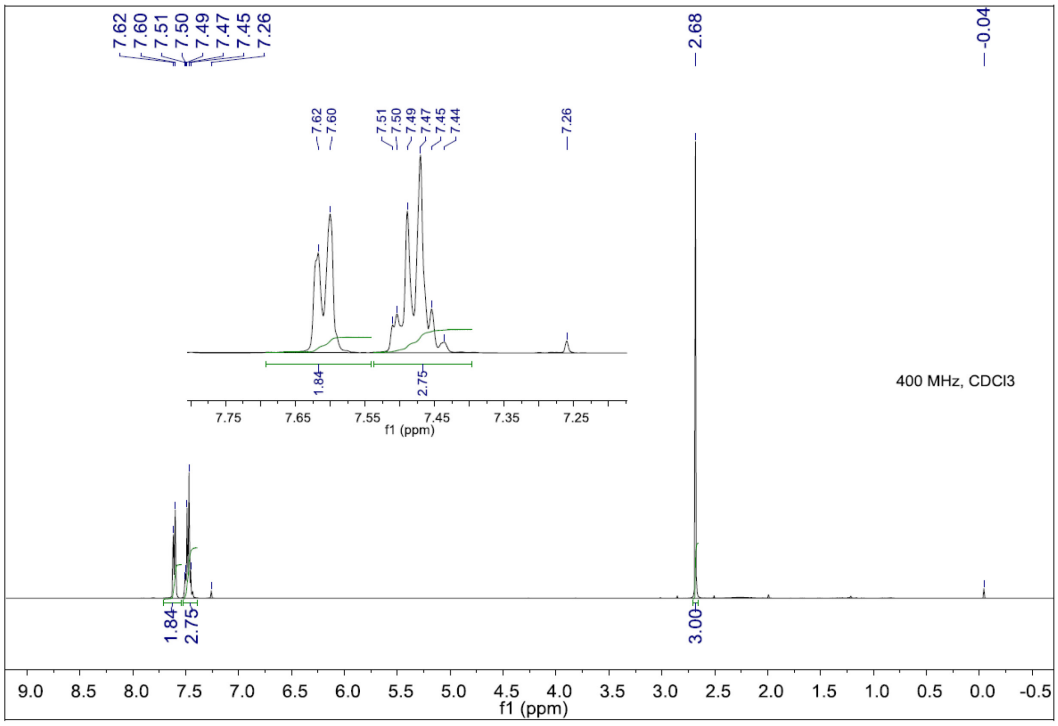

Methylphenyl sulfone: δ (ppm): 7.92 (d, J = 7.5 Hz, 2H), 7.66-7.54 (m, 3H), 3.04 (s, 3H)

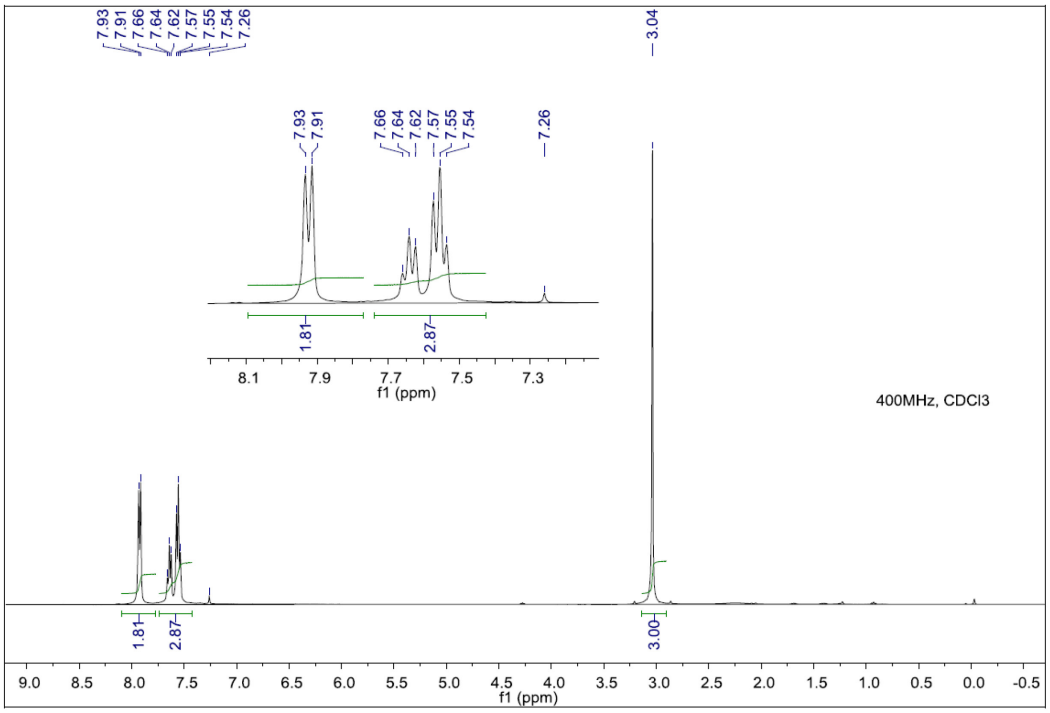

5. Conclusions and future outlooks

In this thesis, we were able to synthesize a novel graphene derivative bearing COOH functions, the graphene acetic acid, employing a scalable and green synthetic route starting from commercial fluorographite. Our synthesis can be considered a big step towards the development of sustainable functionalized graphene materials, since it does not make use of toxic or harmful reagents and can be conducted in environment friendly solvents like anisole and water. Furthermore, with respect to other similar derivatives, our process is carried out at lower temperatures. The structural and chemical propertied of GAA were characterized by various techniques, which ultimately confirmed the presence of extended sp^2 domains interrupted by sp^3 carbon atoms that covalently bind CH_2COOH groups. Moreover, EPR measurements clearly demonstrated the existence of a significant amount of electronic defects, i.e. unpaired electron likely localized at the edges in the material. Thanks to the new synthesis, which is safe, cheap and easily scalable, we could start a more systematic investigation of the catalytic applications of this novel material.

In particular, we started to explore the application of GAA as carbocatalyst for two prototypical reactions: the oxidative homocoupling of primary amines to imines, and the oxidation of sulfides to sulfoxides and sulfones. For the former, we used substituted benzylamine as substrates, obtaining decent conversions in neat conditions at 90°C using molecular oxygen from the air as the final oxidant. We encountered unexpected difficulties during the catalytic tests, especially regarding the accurate evaluation of the conversion, due to the high volatility of the catalytic substrate during reaction conditions and/or problems with the internal standard used for the NMR measurements. More work has to be done, in particular it should be possible to perform the reaction in a closed reactor saturated with oxygen to prevent

the evaporation or to use a technique alternative to NMR (e.g. GC/MS) for the quantification of the products. Despite the practical problems, we were able to obtain a significant insight on the reaction mechanism. We believe that both the spin defects trapped in the material and its carboxyl groups play a synergistic role in the activation of molecular oxygen and benzylamine towards the homocoupling. Experiments of spin trapping of the radical oxygen species (ROS) on the material are currently undertaken via ESR measurements, in order to better understand the mechanism and shed light on the role of the defects. If the spin are found to be the active species, recycle tests could be helpful to understand whether they are consumed or not during the reaction and if that is the case, what type of treatment would be necessary to reform the defects on the material. Finally, our data suggest that the reaction is thermally activated and the reaction path does not involve the formation of alkyl amines.

For what concerns the oxidation of sulfides, we exploited the GAA for the complete and selective conversion of thioanisole to methylphenyl sulfoxide in 60 minutes, at room temperature using hydrogen peroxide as oxidant. Recycle tests show that the GAA performs as a true catalyst and not as a stoichiometric activator, as confirmed also by XPS measurements indicating that the chemical nature of the GAA remain unaltered after catalysis.

A scope of different substrates is needed to obtain insights on the mechanism of the reaction and determine whether the high selectivity towards the methylphenyl sulfoxide found with thioanisole can be extended to other sulfides. The exact role of GAA is still to be explored via tests at different catalytic loadings and a definitive confirmation about the catalytic mechanism has still to be obtained.

As a whole, the work reported in this thesis confirms the still untapped potential of GAA as a powerful carbocatalyst. Despite the differences in the reactions investigated

and building upon the knowledge acquired previously by the works on the structurally close GA, we can start to discern a general paradigm regarding the GAA catalytic activity. It is quite clear that this material is able to catalyse several redox reactions and in particular, reactions involving the participation of reactive oxygen species. Indeed also the oxidative coupling of amines is thought to involve the superoxide species, which eventually produce in-situ H_2O_2[69]: in this respect, a preliminary spin-trapping ESR experiment on the GAA-benzylamine system with DMPO shows the presence of the DMPO-OH species (see Fig. 36 in the experimental section) which might originate from the degradation of DMPO-OOH, suggesting the formation of the superoxide.

This is made possible by the presence of two factors: an unusually high number of electron defects (unpaired electrons) and a high electron conductivity and electron storage ability. GAA as GA, but at variance with GO, is a good electronic conductor and has excellent redox mediator properties. In the case of GA, this has been directly confirmed theoretically by DFT calculations[45] and experimentally by electrochemical measurements[52]. We expect the same for GAA and preliminary electrochemical experiments demonstrated that this material is highly conductive and endowed with excellent electron transfer properties.

The high electron conduction and presence of electronic defects are key to redox activity since the materials can act as an electron reservoir that can be used on demand in different reaction steps[84,85]. The activation of oxygen and oxygen species is a direct consequence of this ability to easily donate or accept electrons. In this regard we want to mention that preliminary studies on GAA as a peroxidase mimic evidenced an exceptional activity, even higher than that of carboxylated GO[86] despite the presence of the same type of functional groups on the surface, the only difference being the insulating nature of GO vs the highly conductive properties of GAA.

Similarly, GAA has been also tested as an electrocatalysts for the oxygen reduction reaction (i.e. the electrochemical reduction of oxygen to water or hydrogen peroxide), showing once again an extremely high activity in the selective production of hydrogen peroxide.

On the other hand, the reason for the presence of unpaired electrons in GAA can be related to the extended defluorination reactions that are involved during their synthesis and the concurrent rehybridization of C form sp^3 to sp^2.

Finally, we want to mention another interesting opportunity offered by GAA, which is the exploitation of its carboxylic group to bind covalently molecular catalysts that in this way not only can be effectively heterogenized, imparting stability easy separation and recyclability, but also acquire good electron conduction properties and be used to catalyse photo or electrochemical reactions. This strategy has been already explored in the case of GA[87] and other carbon nanomaterials (i.e. oxidized nanotubes) and we expect to be equally feasible and advantageous, with the additional benefit of a material that is much cheaper and easier to synthesize.

Bibliography

1. Anastas, P. T. & Williamson, T. C. Green Chemistry: An Overview. in *ACS Symposium Series* vol. 626 1–17 (1996).

2. Anastas, P. & Eghbali, N. Green Chemistry: Principles and Practice. *Chem. Soc. Rev.* **39**, 301–312 (2010).

3. Pop, E., Varshney, V. & Roy, A. K. Thermal properties of graphene: Fundamentals and applications. *MRS Bull.* **37**, 1273–1281 (2012).

4. Papageorgiou, D. G., Kinloch, I. A. & Young, R. J. Mechanical properties of graphene and graphene-based nanocomposites. *Prog. Mater. Sci.* **90**, 75–127 (2017).

5. Castro Neto, A. H., Guinea, F., Peres, N. M. R., Novoselov, K. S. & Geim, A. K. The electronic properties of graphene. *Rev. Mod. Phys.* **81**, 109–162 (2009).

6. Zhu, Y., Ji, H., Cheng, H. M. & Ruoff, R. S. Mass production and industrial applications of graphene materials. *Natl. Sci. Rev.* **5**, 90–101 (2018).

7. Sun, Y., Sun, M. & Xie, D. Graphene Electronic Devices. *Graphene Fabr. Charact. Prop. Appl.* 103–155 (2018) doi:10.1016/B978-0-12-812651-6.00005-7.

8. Novoselov, K. S. *et al.* Electric field in atomically thin carbon films. *Science (80-.).* **306**, 666–669 (2004).

9. Su, C. Y. *et al.* High-quality thin graphene films from fast electrochemical exfoliation. *ACS Nano* **5**, 2332–2339 (2011).

10. Mishra, N., Boeckl, J., Motta, N. & Iacopi, F. Graphene growth on silicon

carbide: A review. *Phys. status solidi* **213**, 2277–2289 (2016).

11. Zhang, Y., Zhang, L. & Zhou, C. Review of Chemical Vapor Deposition of Graphene and Related Applications. *Acc. Chem. Res.* **46**, 2329–2339 (2013).

12. Mbayachi, V. B. *et al.* Graphene synthesis, characterization and its applications: A review. *Results Chem.* **3**, 100163 (2021).

13. Kuila, T. *et al.* Chemical functionalization of graphene and its applications. *Prog. Mater. Sci.* **57**, 1061–1105 (2012).

14. Stankovich, S. *et al.* Graphene-based composite materials. *Nature* **442**, 282–286 (2006).

15. Jung, I., Dikin, D. A., Piner, R. D. & Ruoff, R. S. Tunable Electrical Conductivity of Individual Graphene Oxide Sheets Reduced at 'Low' Temperatures. *NANO Lett.* **8**, 4283–4287 (2008).

16. Jung, I. *et al.* Characterization of Thermally Reduced Graphene Oxide by Imaging Ellipsometry. *J. Phys. Chem. C* **112**, 8499–8506 (2008).

17. Tarcan, R. *et al.* Reduced graphene oxide today. *Journal of Materials Chemistry C* vol. 8 1198–1224 at https://doi.org/10.1039/c9tc04916a (2020).

18. De Silva, K. K. H., Huang, H. H., Joshi, R. K. & Yoshimura, M. Chemical reduction of graphene oxide using green reductants. *Carbon N. Y.* **119**, 190–199 (2017).

19. An, S. J. *et al.* Thin Film Fabrication and Simultaneous Anodic Reduction of Deposited Graphene Oxide Platelets by Electrophoretic Deposition. *J. Phys. Chem. Lett.* **1**, 1259–1263 (2010).

20. Zhan, D. *et al.* Electronic structure of graphite oxide and thermally reduced

graphite oxide. *Carbon N. Y.* **49**, 1362–1366 (2011).

21. Boukhvalov, D. W. & Katsnelson, M. I. Modeling of Graphite Oxide. *J. Am. Chem. Soc.* **130**, 10697–10701 (2008).

22. McCoy, T. M., Turpin, G., Teo, B. M. & Tabor, R. F. Graphene oxide: a surfactant or particle? *Curr. Opin. Colloid Interface Sci.* **39**, 98–109 (2019).

23. Georgakilas, V. *et al.* Functionalization of Graphene: Covalent and Non-Covalent Approaches, Derivatives and Applications. *Chem. Rev.* **112**, 6156–6214 (2012).

24. Wang, H., Maiyalagan, T. & Wang, X. Review on Recent Progress in Nitrogen-Doped Graphene: Synthesis, Characterization, and Its Potential Applications. *ACS Catal.* **2**, 781–794 (2012).

25. Agnoli, S. & Favaro, M. Doping graphene with boron: a review of synthesis methods, physicochemical characterization, and emerging applications. *J. Mater. Chem. A* **4**, 5002–5025 (2016).

26. Yang, Z. *et al.* Sulfur-doped graphene as an efficient metal-free cathode catalyst for oxygen reduction. *ACS Nano* **6**, 205–11 (2012).

27. Wen, Y., Wang, B., Huang, C., Wang, L. & Hulicova-Jurcakova, D. Synthesis of Phosphorus-Doped Graphene and its Wide Potential Window in Aqueous Supercapacitors. *Chem. - A Eur. J.* **21**, 80–85 (2015).

28. Wang, Z. *et al.* Synthesis, characterization and electrical properties of silicon-doped graphene films. *J. Mater. Chem. C* **3**, 6301–6306 (2015).

29. Giovannetti, G. *et al.* Doping graphene with metal contacts. *Phys. Rev. Lett.* **101**, 026803 (2008).

30. Paulus, G. L. C., Wang, Q. H. & Strano, M. S. Covalent electron transfer chemistry of graphene with diazonium salts. *Acc. Chem. Res.* **46**, 160–70 (2013).

31. Xu, Y. *et al.* A Graphene Hybrid Material Covalently Functionalized with Porphyrin: Synthesis and Optical Limiting Property. *Adv. Mater.* **21**, 1275–1279 (2009).

32. Liu, Z., Robinson, J. T., Sun, X. & Dai, H. PEGylated nanographene oxide for delivery of water-insoluble cancer drugs. *J. Am. Chem. Soc.* **130**, 10876–10877 (2008).

33. Georgakilas, V. *et al.* Noncovalent Functionalization of Graphene and Graphene Oxide for Energy Materials, Biosensing, Catalytic, and Biomedical Applications. *Chem. Rev.* **116**, 5464–5519 (2016).

34. Tan, C., Huang, X. & Zhang, H. Synthesis and applications of graphene-based noble metal nanostructures. *Mater. Today* **16**, 29–36 (2013).

35. Favaro, M. *et al.* TiO2/graphene nanocomposites from the direct reduction of graphene oxide by metal evaporation. *Carbon N. Y.* **68**, 319–329 (2014).

36. Mosconi, D. *et al.* One-pot synthesis of MoS 2(1–x) Se 2x on N-doped reduced graphene oxide: tailoring chemical and structural properties for photoenhanced hydrogen evolution reaction. *Nanoscale Adv.* **2**, 4830–4840 (2020).

37. Chang, H. & Wu, H. Graphene-Based Nanomaterials: Synthesis, Properties, and Optical and Optoelectronic Applications. *Adv. Funct. Mater.* **23**, 1984–1997 (2013).

38. Ruff, O. & Bretschneider, O. Die Reaktionsprodukte der verschiedenen

Kohlenstoffformen mit Fluor II (Kohlenstoff-monofluorid). *Zeitschrift fur Anorg. und Allg. Chemie* **217**, 1–18 (1934).

39. Robinson, J. T. *et al.* Properties of Fluorinated Graphene Films. *Nano Lett.* **10**, 3001–3005 (2010).

40. Zbořil, R. *et al.* Graphene Fluoride: A Stable Stoichiometric Graphene Derivative and its Chemical Conversion to Graphene. *Small* **6**, 2885–2891 (2010).

41. O'Hagan, D. Understanding organofluorine chemistry. An introduction to the C–F bond. *Chem. Soc. Rev.* **37**, 308–319 (2008).

42. Liang, Y. & Yang, L. Electronic Structure and Optical Absorption of Fluorographene. *MRS Proc.* **1370**, mrss11-1370-yy04-02 (2011).

43. Karlický, F. & Otyepka, M. Band Gaps and Optical Spectra of Chlorographene, Fluorographene and Graphane from G 0 W 0 , GW 0 and GW Calculations on Top of PBE and HSE06 Orbitals. *J. Chem. Theory Comput.* **9**, 4155–4164 (2013).

44. Whitener, K. E., Stine, R., Robinson, J. T. & Sheehan, P. E. Graphene as electrophile: Reactions of graphene fluoride. *J. Phys. Chem. C* **119**, 10507–10512 (2015).

45. Bakandritsos, A. *et al.* Cyanographene and Graphene Acid: Emerging Derivatives Enabling High-Yield and Selective Functionalization of Graphene. *ACS Nano* **11**, 2982–2991 (2017).

46. Hummers, W. S. & Offeman, R. E. Preparation of Graphitic Oxide. *J. Am. Chem. Soc.* **80**, 1339–1339 (1958).

47. Eng, A. Y. S., Chua, C. K. & Pumera, M. Refinements to the structure of

graphite oxide: absolute quantification of functional groups via selective labelling. *Nanoscale* **7**, 20256–20266 (2015).

48. Andre Mkhoyan, K. *et al.* Atomic and electronic structure of graphene-oxide. *Nano Lett.* **9**, 1058–63 (2009).

49. Jankovský, O. *et al.* A New Member of the Graphene Family: Graphene Acid. *Chem. - A Eur. J.* **22**, 17416–17424 (2016).

50. Blanco, M., Agnoli, S. & Granozzi, G. Graphene Acid: A Versatile 2D Platform for Catalysis. *Isr. J. Chem.* **62**, (2022).

51. Lerf, A., He, H., Forster, M. & Klinowski, J. Structure of graphite oxide revisited. *J. Phys. Chem. B* **102**, 4477–4482 (1998).

52. Mosconi, D. *et al.* Arene C–H insertion catalyzed by ferrocene covalently heterogenized on graphene acid. *Carbon N. Y.* **143**, 318–328 (2019).

53. Ma, B. *et al.* Hybridization of Molecular and Graphene Materials for CO 2 Photocatalytic Reduction with Selectivity Control. *J. Am. Chem. Soc.* **143**, 8414–8425 (2021).

54. Blanco, M. *et al.* Palladium nanoparticles supported on graphene acid: a stable and eco-friendly bifunctional C–C homo- and cross-coupling catalyst. *Green Chem.* **21**, 5238–5247 (2019).

55. Zaoralová, D., Mach, R., Lazar, P., Medveď, M. & Otyepka, M. Anchoring of Transition Metals to Graphene Derivatives as an Efficient Approach for Designing Single-Atom Catalysts. *Adv. Mater. Interfaces* **8**, 2001392 (2021).

56. Konwar, L. J., Boro, J. & Deka, D. Review on latest developments in biodiesel production using carbon-based catalysts. *Renew. Sustain. Energy Rev.* **29**, 546–

564 (2014).

57. Dreyer, D. R., Jia, H.-P. & Bielawski, C. W. Graphene Oxide: A Convenient Carbocatalyst for Facilitating Oxidation and Hydration Reactions. *Angew. Chemie Int. Ed.* **49**, n/a-n/a (2010).

58. Presolski, S. & Pumera, M. Graphene Oxide: Carbocatalyst or Reagent? *Angew. Chemie* **130**, 16955–16957 (2018).

59. Blanco, M. *et al.* Combined high degree of carboxylation and electronic conduction in graphene acid sets new limits for metal free catalysis in alcohol oxidation. *Chem. Sci.* **10**, 9438–9445 (2019).

60. Long, J. *et al.* Nitrogen-doped graphene nanosheets as metal-free catalysts for aerobic selective oxidation of benzylic alcohols. *ACS Catal.* **2**, 622–631 (2012).

61. Dhakshinamoorthy, A., Primo, A., Concepcion, P., Alvaro, M. & Garcia, H. Doped Graphene as a Metal-Free Carbocatalyst for the Selective Aerobic Oxidation of Benzylic Hydrocarbons, Cyclooctane and Styrene. *Chem. - A Eur. J.* **19**, 7547–7554 (2013).

62. Qiu, H. *et al.* Highly enantioselective trapping of zwitterionic intermediates by imines. *Nat. Chem. 2012 49* **4**, 733–738 (2012).

63. Martin, S. F. Recent Applications of Imines as Key Intermediates in the Synthesis of Alkaloids and Novel Nitrogen Heterocycles. *Pure Appl. Chem.* **81**, 195 (2009).

64. Murahashi, S. -I. Synthetic Aspects of Metal-Catalyzed Oxidations of Amines and Related Reactions. *Angew. Chemie Int. Ed. English* **34**, 2443–2465 (1995).

65. Layer, R. W. The chemistry of imines. *Chem. Rev.* **63**, 489–510 (1963).

66. Dai, L. X. Stereoselective reactions with imines. *Pure Appl. Chem.* **71**, 1033–1040 (1999).

67. Largeron, M. Novel Protocols for the Catalytic Oxidation of Primary Amines to Imines. doi:10.1002/ejoc.200((will).

68. Liu, L., Zhang, S., Fu, X. & Yan, C.-H. Metal-free aerobic oxidative coupling of amines to imines. *Chem. Commun.* **47**, 10148 (2011).

69. Su, C. *et al.* Probing the catalytic activity of porous graphene oxide and the origin of this behaviour. *Nat. Commun. 2012 31* **3**, 1–9 (2012).

70. Fernández, I. & Khiar, N. Recent developments in the synthesis and utilization of chiral sulfoxides. *Chem. Rev.* **103**, 3651–3705 (2003).

71. Sago, J. & Hall, R. P. Dapsone. *Dermatol. Ther.* **15**, 340–351 (2002).

72. Deberdeev, T. R. *et al.* Aromatic Polysulfones: Strategies of Synthesis, Properties, and Application. *Polym. Sci. - Ser. D* **13**, 320–328 (2020).

73. Rayner, C. M. Synthesis of thiols, sulfides, sulfoxides and sulfones. *Contemp. Org. Synth.* **2**, 409 (1995).

74. Golchoubian, H. & Hosseinpoor, F. Effective oxidation of sulfides to sulfoxides with hydrogen peroxide under transition-metal-free conditions. *Molecules* **12**, 304–311 (2007).

75. Marcano, D. C. *et al.* Improved Synthesis of Graphene Oxide. *ACS Nano* **4**, 4806–4814 (2010).

76. Abdi, G., Alizadeh, A. & Khodaei, M. M. Highly carboxyl-decorated graphene oxide sheets as metal-free catalytic system for chemoselective oxidation of sulfides to sulfones. *Mater. Chem. Phys.* **201**, 323–330 (2017).

77. Wang, X. *et al.* Controllable defluorination of fluorinated graphene and weakening of C–F bonding under the action of nucleophilic dipolar solvent. *Phys. Chem. Chem. Phys.* **18**, 3285–3293 (2016).

78. Henderson, R. K. *et al.* Expanding GSK's solvent selection guide – embedding sustainability into solvent selection starting at medicinal chemistry. *Green Chem.* **13**, 854–862 (2011).

79. Yeh, J. J. & Lindau, I. Atomic subshell photoionization cross sections and asymmetry parameters: $1 \leqslant Z \leqslant 103$. *At. Data Nucl. Data Tables* **32**, 1–155 (1985).

80. Tanuma, S., Powell, C. J. & Penn, D. R. Calculations of electron inelastic mean free paths. IX. Data for 41 elemental solids over the 50 eV to 30 keV range. *Surf. Interface Anal.* **43**, 689–713 (2011).

81. Gupta, B. *et al.* Role of oxygen functional groups in reduced graphene oxide for lubrication. *Sci. Reports 2017 71* **7**, 1–14 (2017).

82. Diamantopoulou, A., Glenis, S., Zolnierkiwicz, G., Guskos, N. & Likodimos, V. Magnetism in pristine and chemically reduced graphene oxide. *J. Appl. Phys.* **121**, 043906 (2017).

83. Horsley, L. H. Table of Azeotropes and Nonazeotropes. *Anal. Chem.* **19**, 508–600 (1947).

84. Larsen, J. W., Freund, M., Kim, K. Y., Sidovar, M. & Stuart, J. L. Mechanism of the carbon catalyzed reduction of nitrobenzene by hydrazine. *Carbon N. Y.* **38**, 655–661 (2000).

85. Blanco, M. *et al.* Positive and negative regulation of carbon nanotube catalysts

through encapsulation within macrocycles. *Nat. Commun. 2018 91* **9**, 1–7 (2018).

86. Song, Y., Qu, K., Zhao, C., Ren, J. & Qu, X. Graphene Oxide: Intrinsic Peroxidase Catalytic Activity and Its Application to Glucose Detection. *Adv. Mater.* **22**, 2206–2210 (2010).

87. Ma, B. *et al.* Hybridization of Molecular and Graphene Materials for CO2Photocatalytic Reduction with Selectivity Control. *J. Am. Chem. Soc.* **143**, 8414–8425 (2021).